Spiral and Elliptical Galaxies: what are their properties and how did they form?

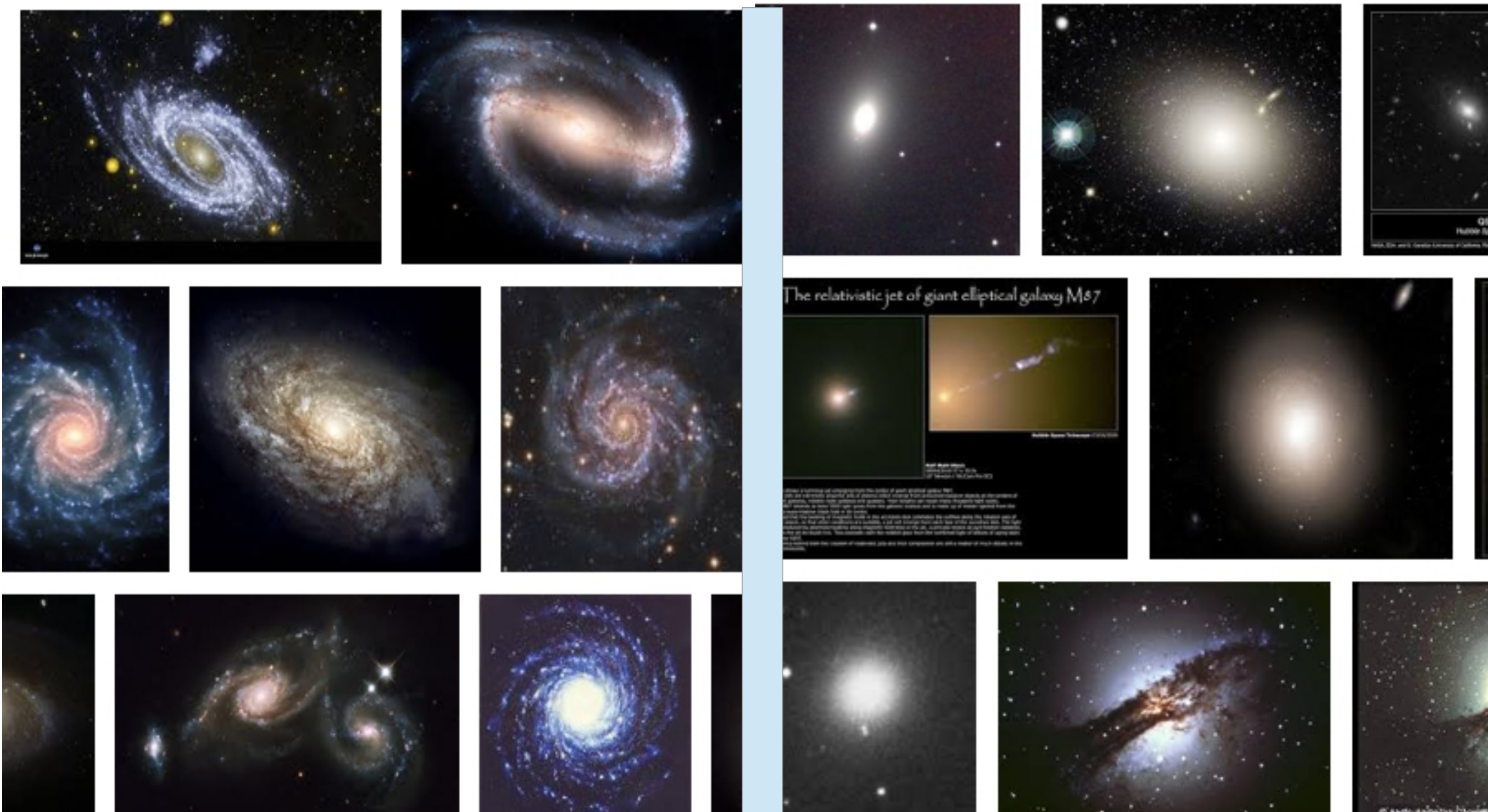

(i) deVaucouleurs ($R^{1/4}$) and Sersic ($R^{1/n}$) Laws

deVaucouleurs noticed (1948) that for many ellipticals $\mu \propto R^{1/4}$
The fit is usually good over all but the inner and outermost regions (typically 0.03 - 20 R_e)

The law is usually written :

$$I(R) = I_e \exp\left(-7.67 \left[(R/R_e)^{1/4} - 1 \right]\right) \qquad (7.3)$$

It has the following properties :

- $L_{tot} = 7.22 \pi R_e^2 I_e$
- $I(0) = 2000\, I_e$
- $< I(<R_e)> = 3.61\, I_e$ (which we abbreviate to $< I_e >$ and equivalently $< \mu_e >$)
- Asymptotically, at small R, $I(R) \propto R^{-0.8}$ while at large R, $I(R) \propto R^{-1.7}$
- In terms of surface brightness: $\mu(R) = \mu_e + 8.325[(R/R_e)^{1/4} - 1] = \mu(0) + 8.325 (R/R_e)^{1/4}$

More Luminous E's are More Concentrated

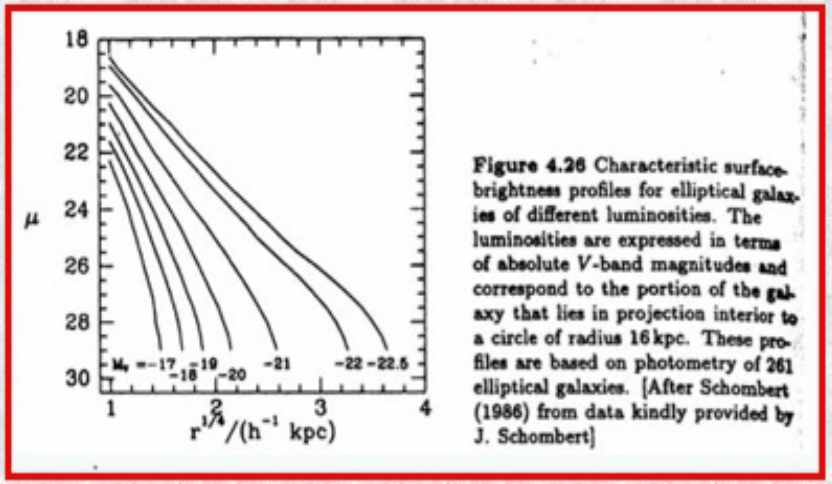

Figure 4.26 Characteristic surface-brightness profiles for elliptical galaxies of different luminosities. The luminosities are expressed in terms of absolute *V*-band magnitudes and correspond to the portion of the galaxy that lies in projection interior to a circle of radius 16 kpc. These profiles are based on photometry of 261 elliptical galaxies. [After Schombert (1986) from data kindly provided by J. Schombert]

Surface brightness profiles for Ellipticals with a range of luminosity. The x axis is $R^{1/4}$ in $kpc^{1/4}$. Clearly, more luminous galaxies are bigger, but also larger n-index since if the profile curves down the n-index is less than 4, but if it curves up it is more than 4.

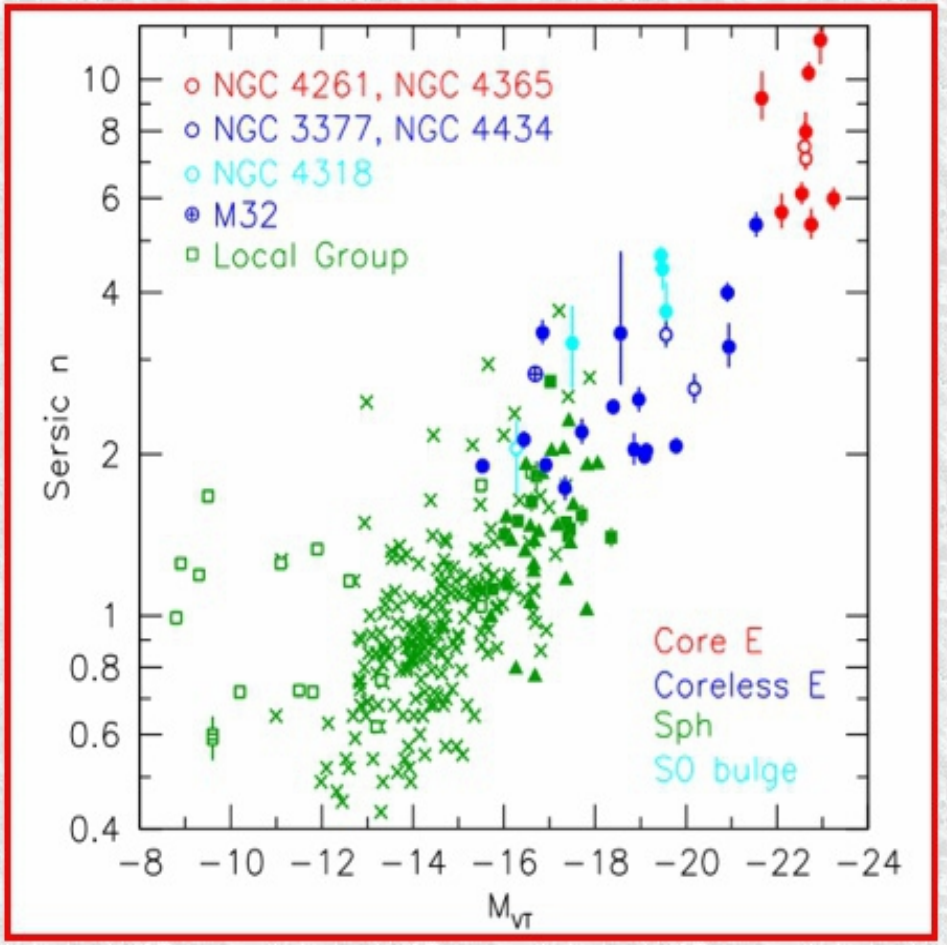

Clear trend for more luminous Elliptical galaxies to have higher n-index (more concentrated profiles). Note the low luminosity dwarf spheroids have Sersic n in the same range as for disks. [Figure 33 from

(ii) Size & Luminosity vs Surface Brightness (Kormendy) Relation

A couple of correlations suggest larger, more luminous galaxies have lower surface brightness

$\langle I_e \rangle$ correlates with R_e : Kormendy Relation

- $R_e \propto \langle I_e \rangle^{-0.83 +/- 0.08}$

$\langle I_e \rangle$ correlates with L_{tot} :

- $L_{tot} \propto \langle I_e \rangle^{-2/3}$
- this follows from the above relation, given $L_e = 1/2\, L_{tot} = \pi \langle I_e \rangle R_e^2$

We conclude: larger and more luminous galaxies are **fluffier** with **lower densities**
An interpretation is not yet too clear, though galaxy formation models must explain it.
One inference: low-luminosity ellipticals formed with more gaseous dissipation than giant ellipticals.

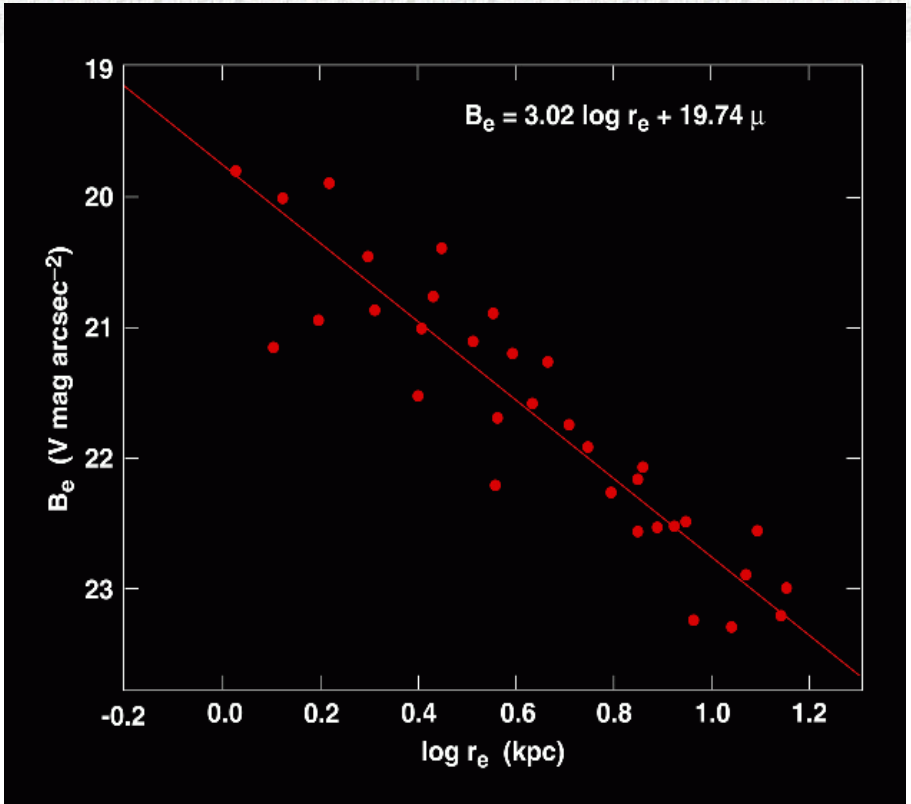

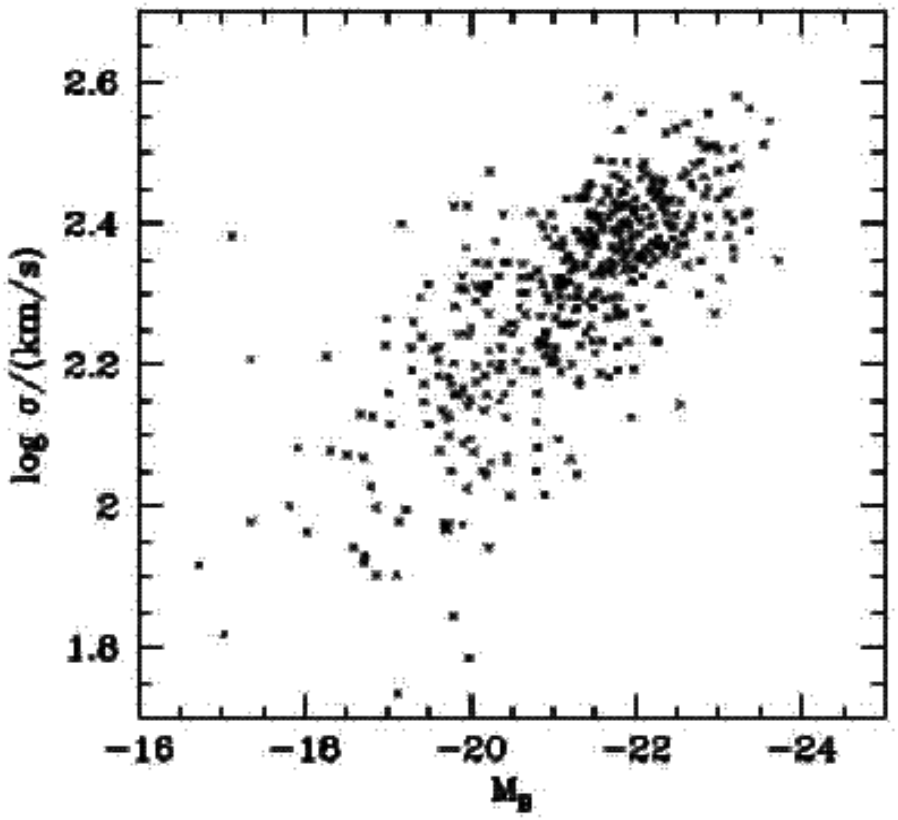

Faber-Jackson relation between central velocity dispersion and total magnitude of elliptical galaxies

$$L_B \propto \sigma^4$$

(b) The 3-Parameter Fundamental Plane

The above 2-parameter correlations have considerable **real scatter**
Furthermore, the residuals in one plot correlate with those in another.
This suggests we look for a tighter correlation among **three** parameters:

- A tilted **plane** of points in 3-D volume, which
- Projects onto 2-D planes as the (looser) correlations seen above
- One example is: $\text{Log } R_e = a \text{ Log } \sigma + b \text{ Log } I_e + c$

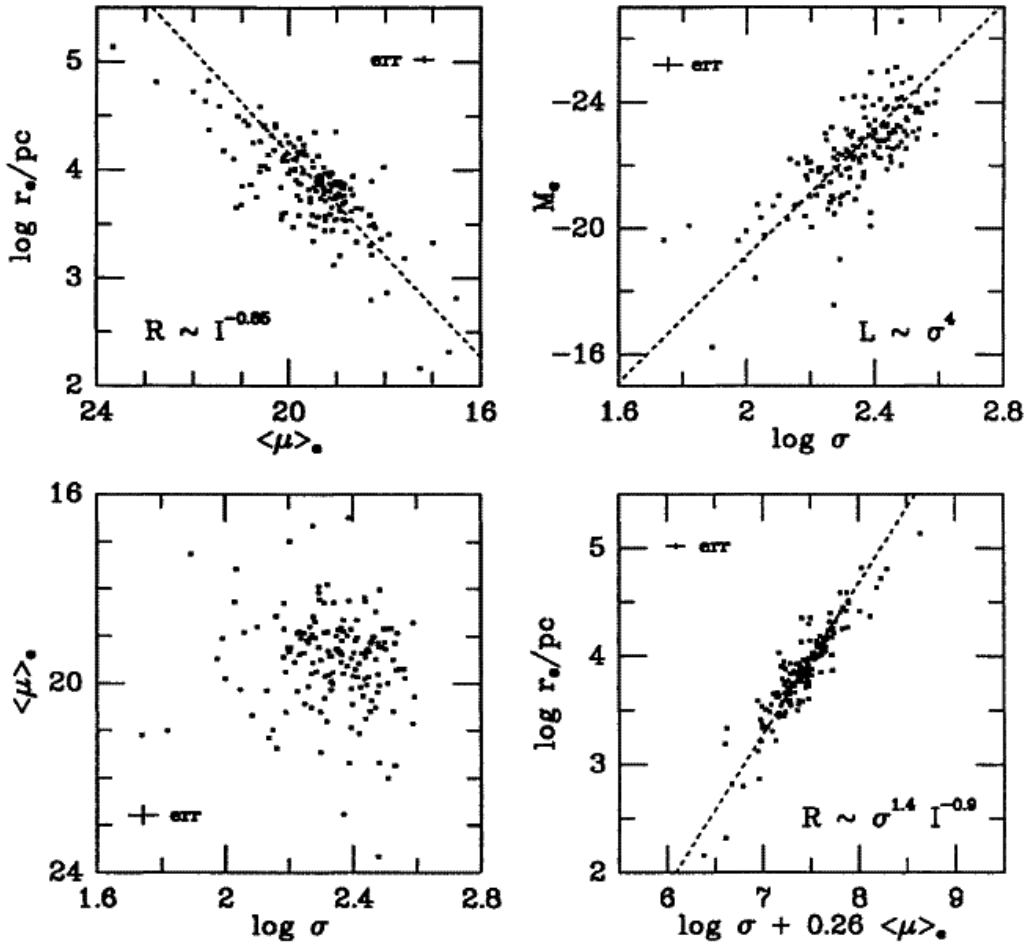

Figure 2 Projections of the fundamental parameter plane of elliptical galaxies. *Top panels*:

(iv) The Physical Basis of the Fundamental Plane

The following gives some insight into the origin of the F-P relation :
Consider:

- $\langle I_e \rangle = \frac{1}{2} L_{tot} / \pi R_e^2$ (just a definition)
- $M/R_e = c \sigma_e^2$ (virial equilibrium, KE $\propto$ PE; c = "structure parameter" containing all details)

Taken together, these give:

- $R_e = (c/2\pi) (M/L)^{-1} \sigma_e^2 \langle I_e \rangle^{-1}$ or equivalently,
- $\text{Log } R_e = \text{Log } [(c/2\pi) (M/L)^{-1}] + 2 \text{Log } \sigma_e - \text{Log} \langle I_e \rangle$ or
- $\text{Log } R_e = \text{Log } [(c/2\pi) (M/L)^{-1}] + 2 \text{Log } \sigma_e + 0.4 \langle \mu_e \rangle$ (since $\langle \mu_e \rangle = -2.5 \text{Log} \langle I_e \rangle$)

So, **if** c and M/L are constants, then we expect

- $\text{Log } R_e = 2 \text{Log } \sigma_e + 0.4 \langle \mu_e \rangle + \text{Log } [(c/2\pi) (M/L)^{-1}]$

Which is **close to**, but not quite, the F-P relation:

- $\text{Log } R_e = 1.4 \text{Log } \sigma_e + 0.36 \langle \mu_e \rangle + \text{const}$

To bring these into agreement, we require:

- $(2\pi/c) (M/L) \propto M^{1/5} \propto L^{1/4}$

Color-Magnitude Relation

Abell 2218

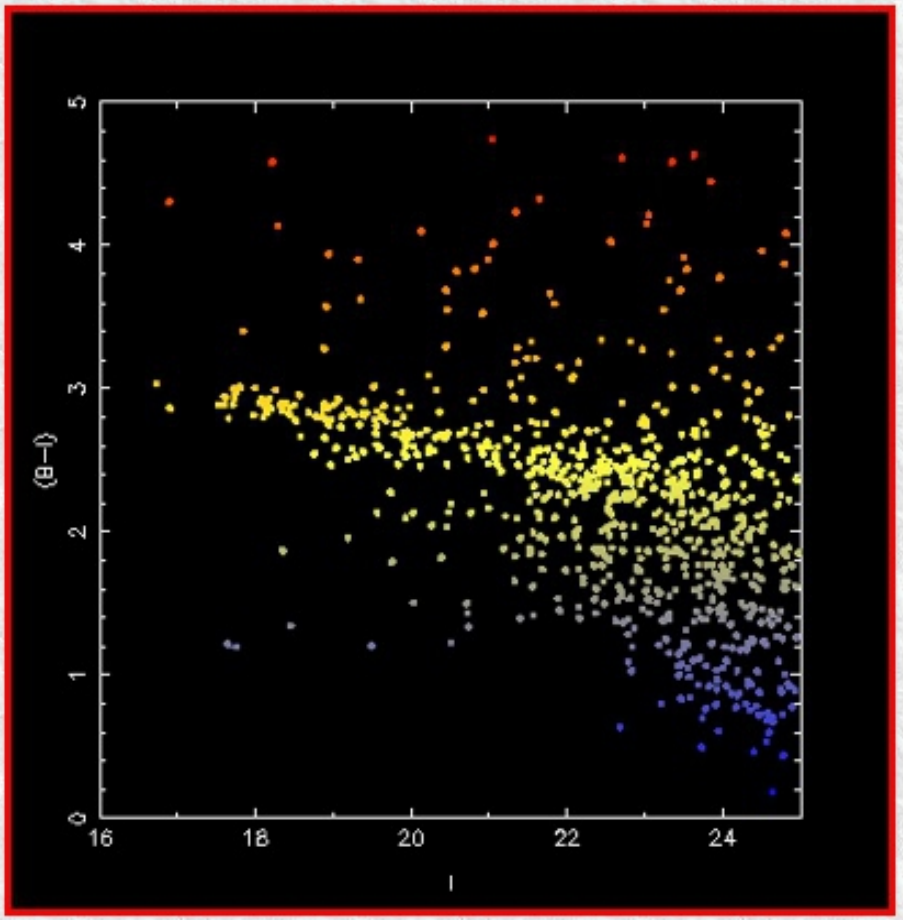

Abell 2218

Colors and magnitude for galaxies in the field of Abell 2218. Many fain background galaxies are included, but the primary early-type color-magnitude strip is clearly visible.

Profile of elliptical galaxies can deviate from the $R^{1/4}$ law at both small and large radius.

Close to the center:

- Some galaxies have **cores** - region where the surface brightness flattens and is ~ constant
- Other galaxies have **cusps** - surface brightness rises steeply as a power-law right to the center

- The **most luminous** ellipticals have cores (typically a slope in the surface brightness distribution $\sim R^{-0.3}$ or flatter)
- **Low luminosity** ellipticals have power law cusps extending inward as far as can be seen
- At intermediate luminosities, mixture of cores and cusps

Results from HST

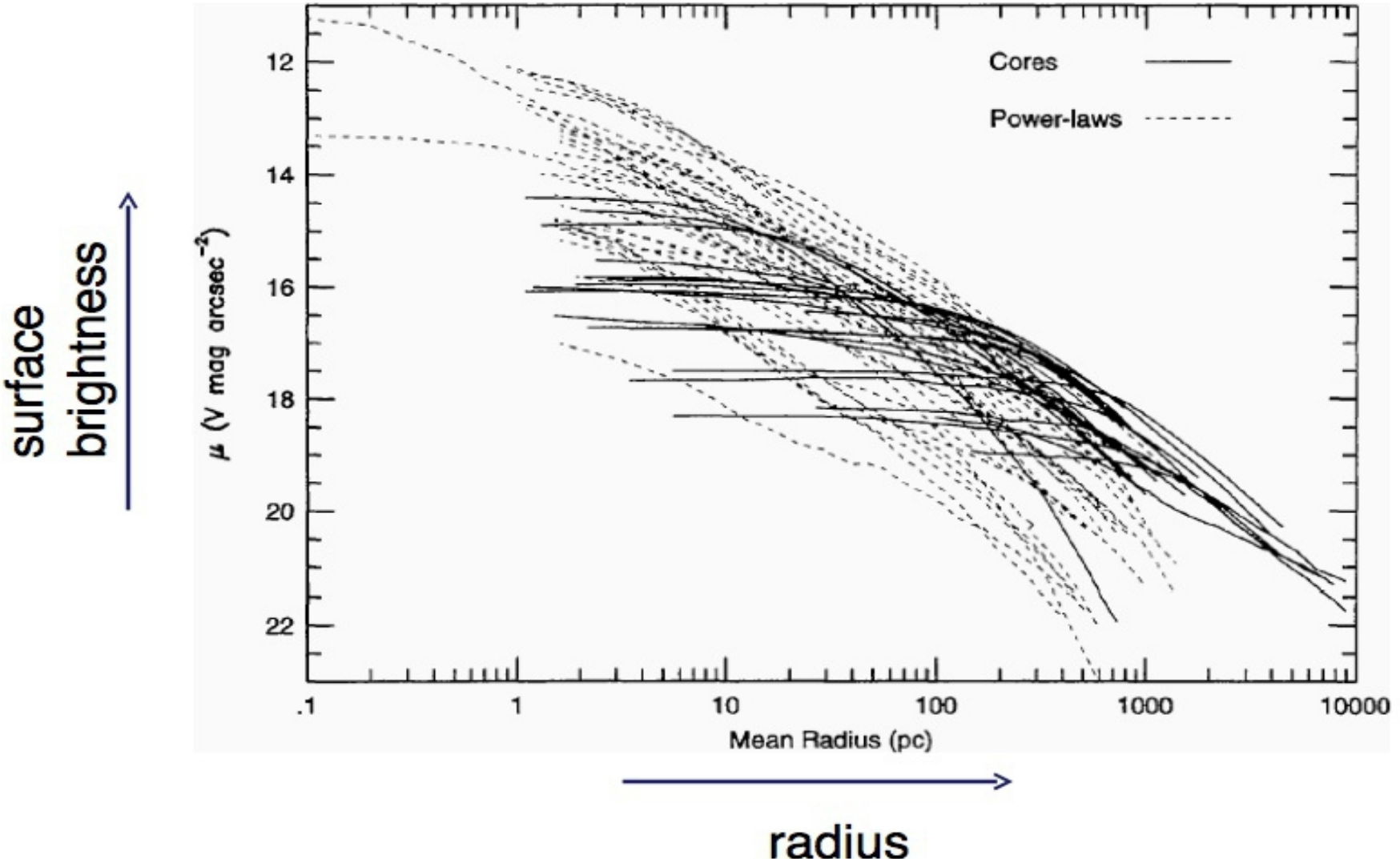

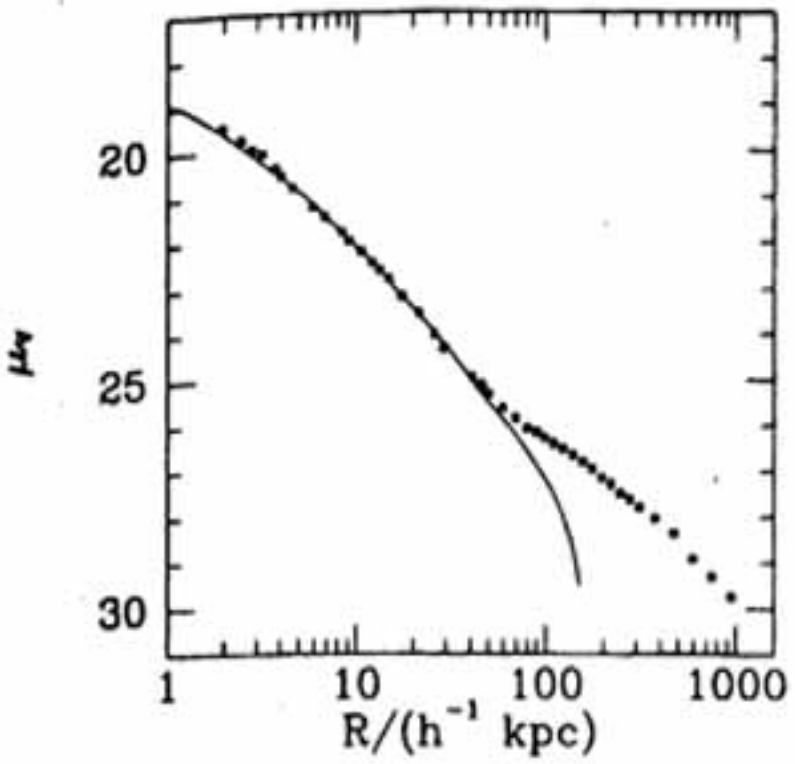

Figure 4.28 The surface-brightness profile of the cD galaxy that lies at the center of the cluster Abell 1413 (points). The line shows the $R^{1/4}$-law that best fits the inner points. [From data kindly provided by J. Schombert based on the work of Oemler (1976).]

Ellipticals with Shells

NGC 3923

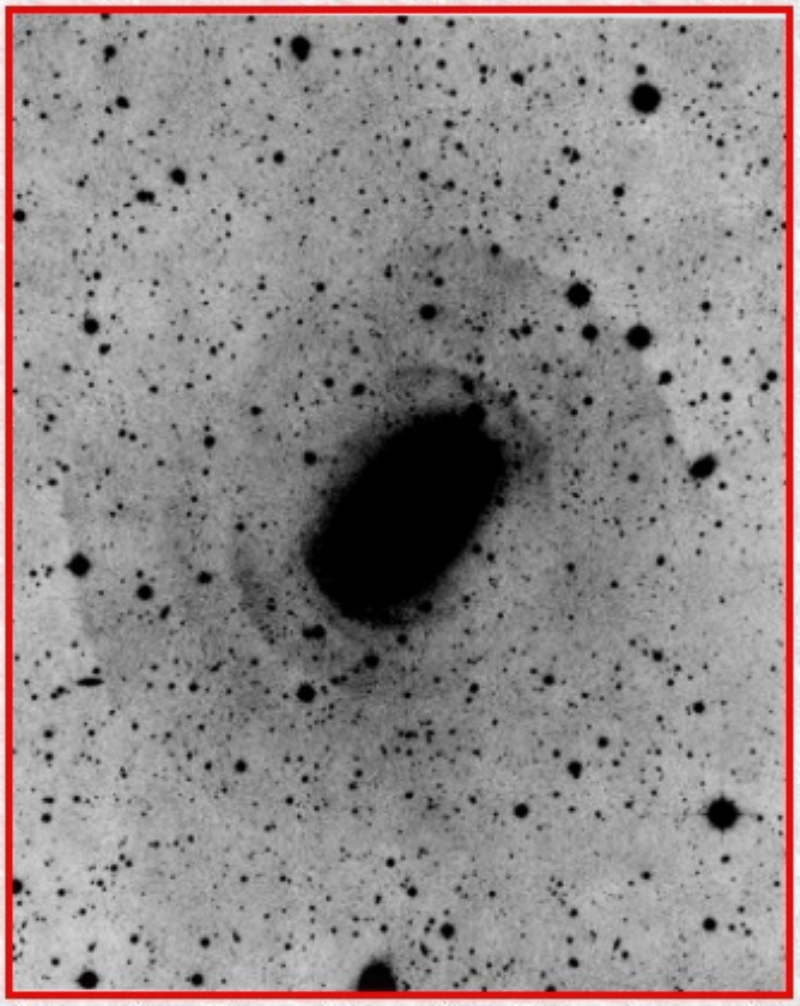

NGC 4382

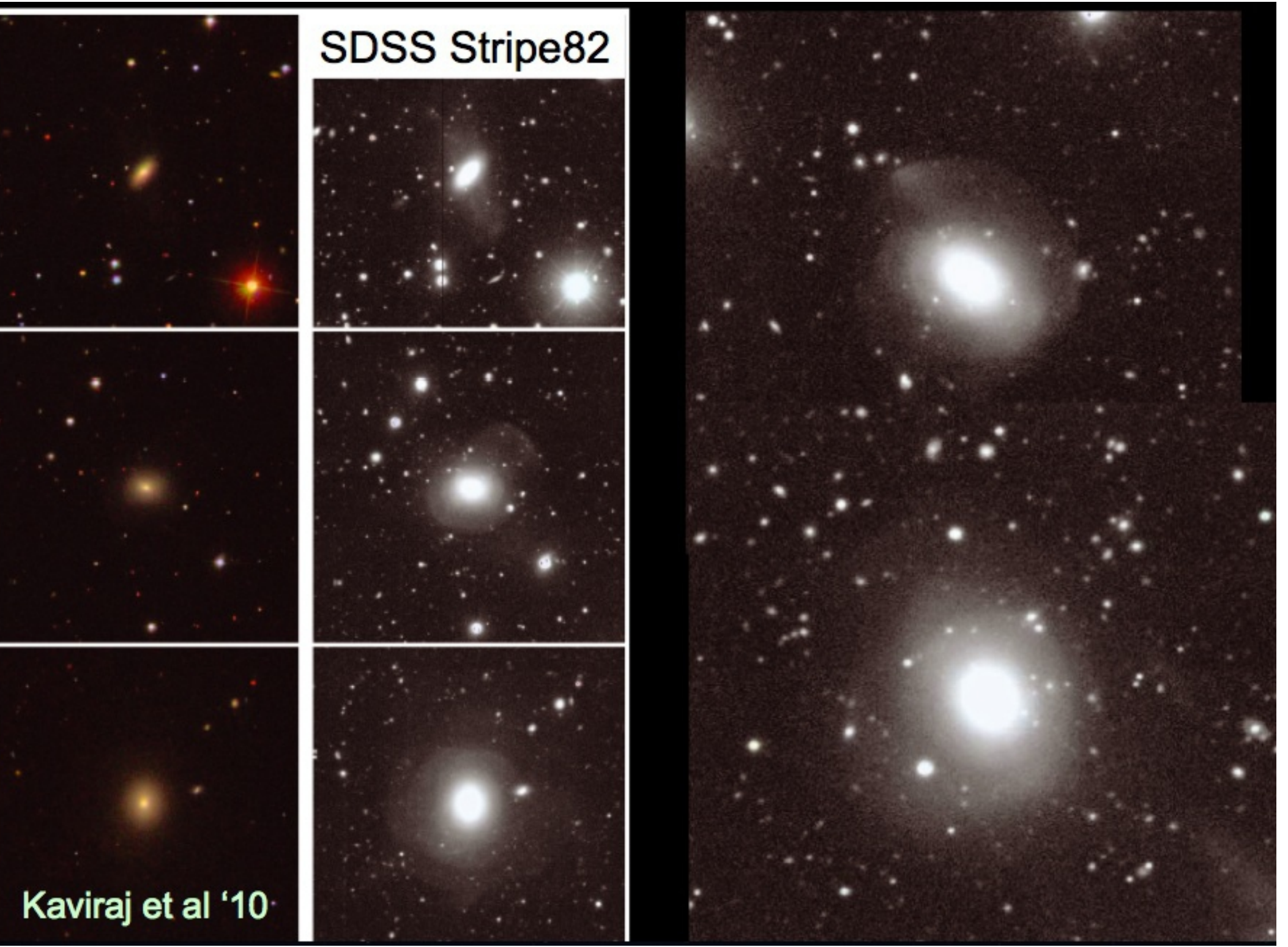
SDSS Stripe82
Kaviraj et al '10

Combine many galaxy images to probe low surface brightness light in outer galaxy

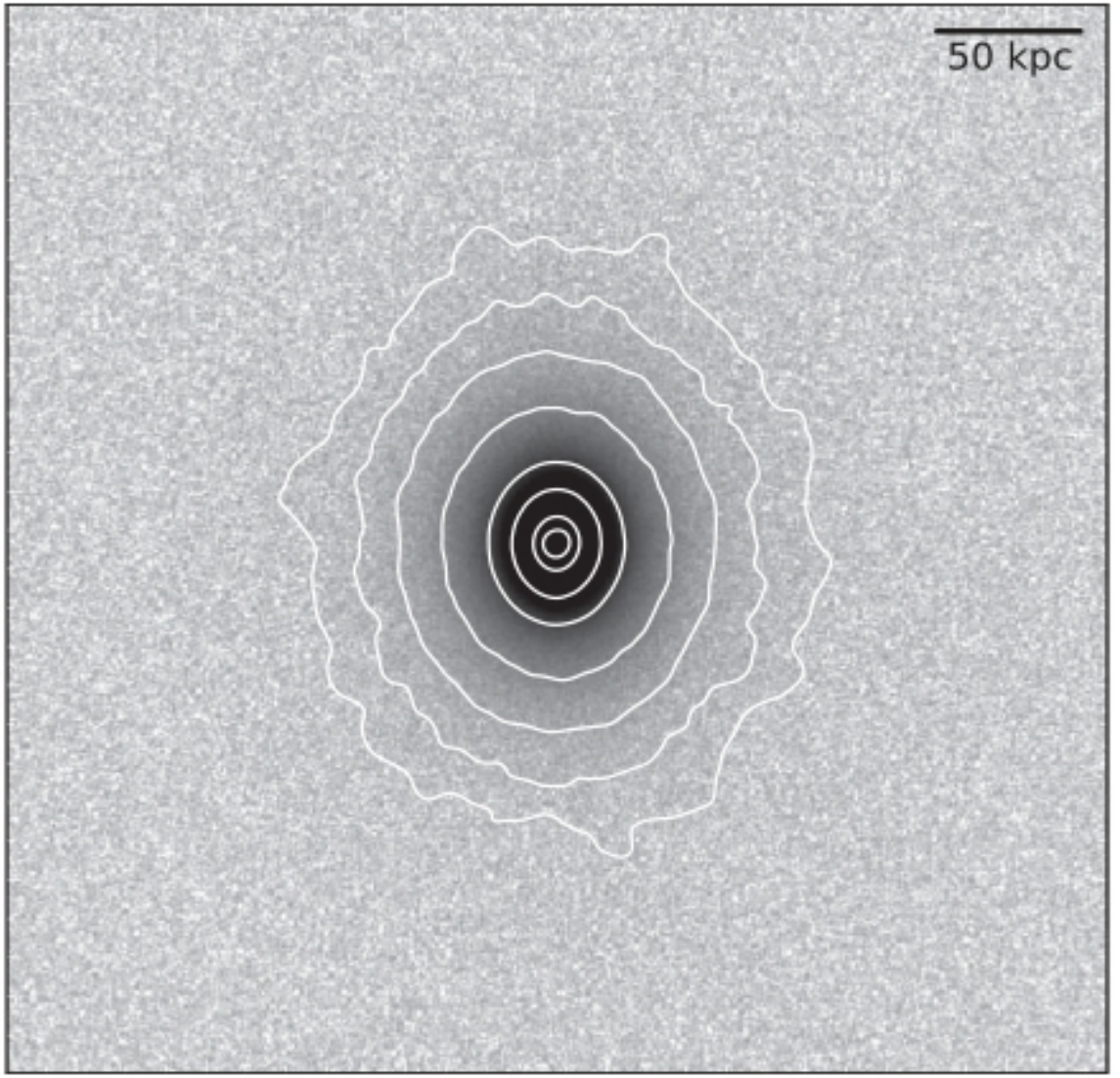

Figure 5. The stacked image consisting of 4040 images in the mass range $10^{11.0}\,M_\odot < M_* < 10^{11.4}\,M_\odot$ and $C > 2.6$. Elliptical contours are drawn at 5, 10, 20, 30, 50, 70, 90 and 110 kpc.

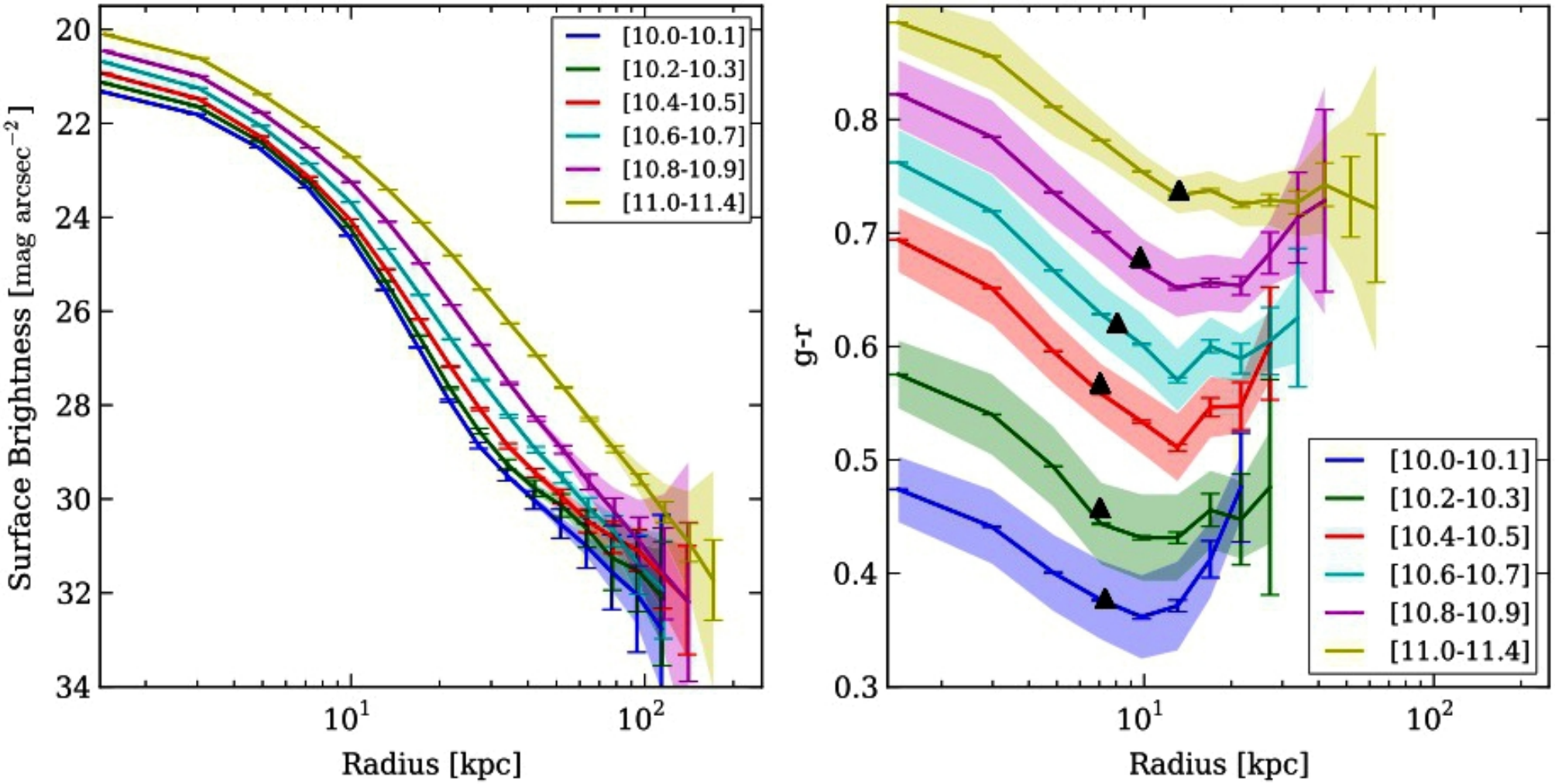
Surface Brightness [mag arcsec^{-2}]
Radius [kpc]
[10.0-10.1]
[10.2-10.3]
[10.4-10.5]
[10.6-10.7]
[10.8-10.9]
[11.0-11.4]
g-r
Radius [kpc]
[10.0-10.1]
[10.2-10.3]
[10.4-10.5]
[10.6-10.7]
[10.8-10.9]
[11.0-11.4]

GALAXY MERGERS AND INTERACTIONS

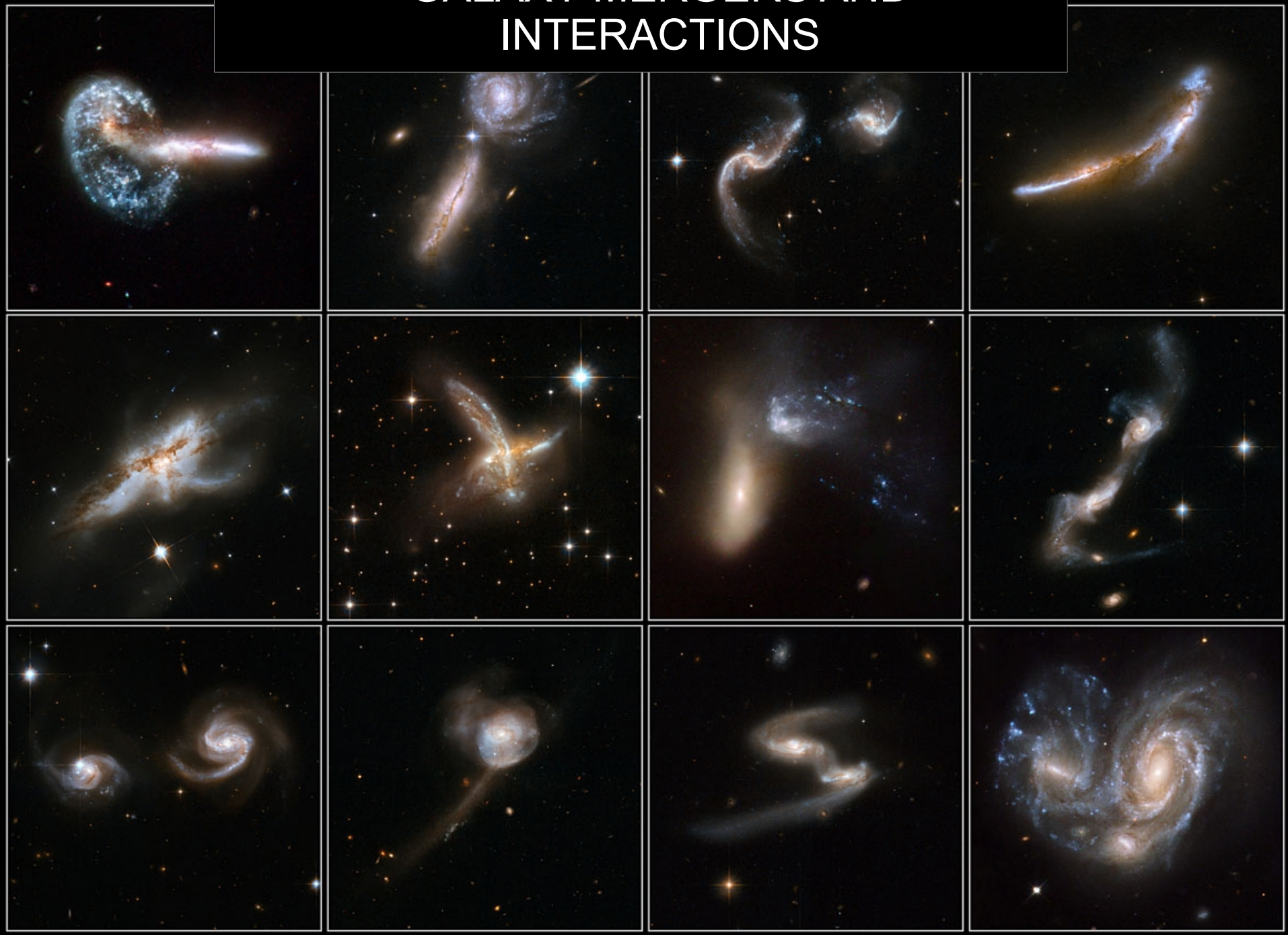

THE ASTROPHYSICAL JOURNAL, 178:623–666, 1972 December 15

GALACTIC BRIDGES AND TAILS

ALAR TOOMRE
Department of Mathematics, Massachusetts Institute of Technology
AND
JURI TOOMRE*
Department of Mathematics, New York University, and
Goddard Institute for Space Studies, New York
Received 1972 May 19

ABSTRACT

This paper argues that the bridges and tails seen in some multiple galaxies are just tidal relics of close encounters. These consequences of the brief but violent tidal forces are here studied in a deliberately simple-minded fashion: Each encounter is considered to involve only two galaxies and to be roughly parabolic; each galaxy is idealized as just a disk of noninteracting test particles which initially orbit a central mass point.

As shown here, the two-sided distortions provoked by gravity alone in such circumstances can indeed evolve kinematically into some remarkably narrow and elongated features: (i) After a relatively direct passage of a *small* companion, the outer portions of the primary disk often deform both into a near-side spiral arm or "bridge" extending toward this satellite, and into a far-side "counterarm." (ii) A similar encounter with an *equal* or more massive partner results typically in a long and curving "tail" of escaping debris from the far side of the victim disk, and in an avalanche of near-side particles, most of which are captured by the satellite.

Besides extensive pictorial surveys of such tidal damage, this paper offers reconstructions of the orbits and *outer* shapes of four specific interacting pairs: Arp 295, M51 + NGC 5195, NGC 4676, and NGC 4038/9. Those models can be found in the fairly self-explanatory figures 19, 21, 22, and 23.

Our present demonstrations will actually share the foremost of those flaws with Pfleiderer and Siedentopf: Like their examples, ours will be based exclusively on restricted three-body computations performed with massless particles which we pretend constitute the outer disks of pairwise interacting galaxies. By supposing these elements of either disk to move simply under inverse-square forces from the two mass points representing the bulk of each galaxy, we too will ignore all explicit self-gravity of the disk material (except in certain final estimates). Obviously this is an important sin of omission, and it is one which ought soon to be remedied, perhaps via some proper N-body calculations.

Retrograde encounters produce only small perturbations

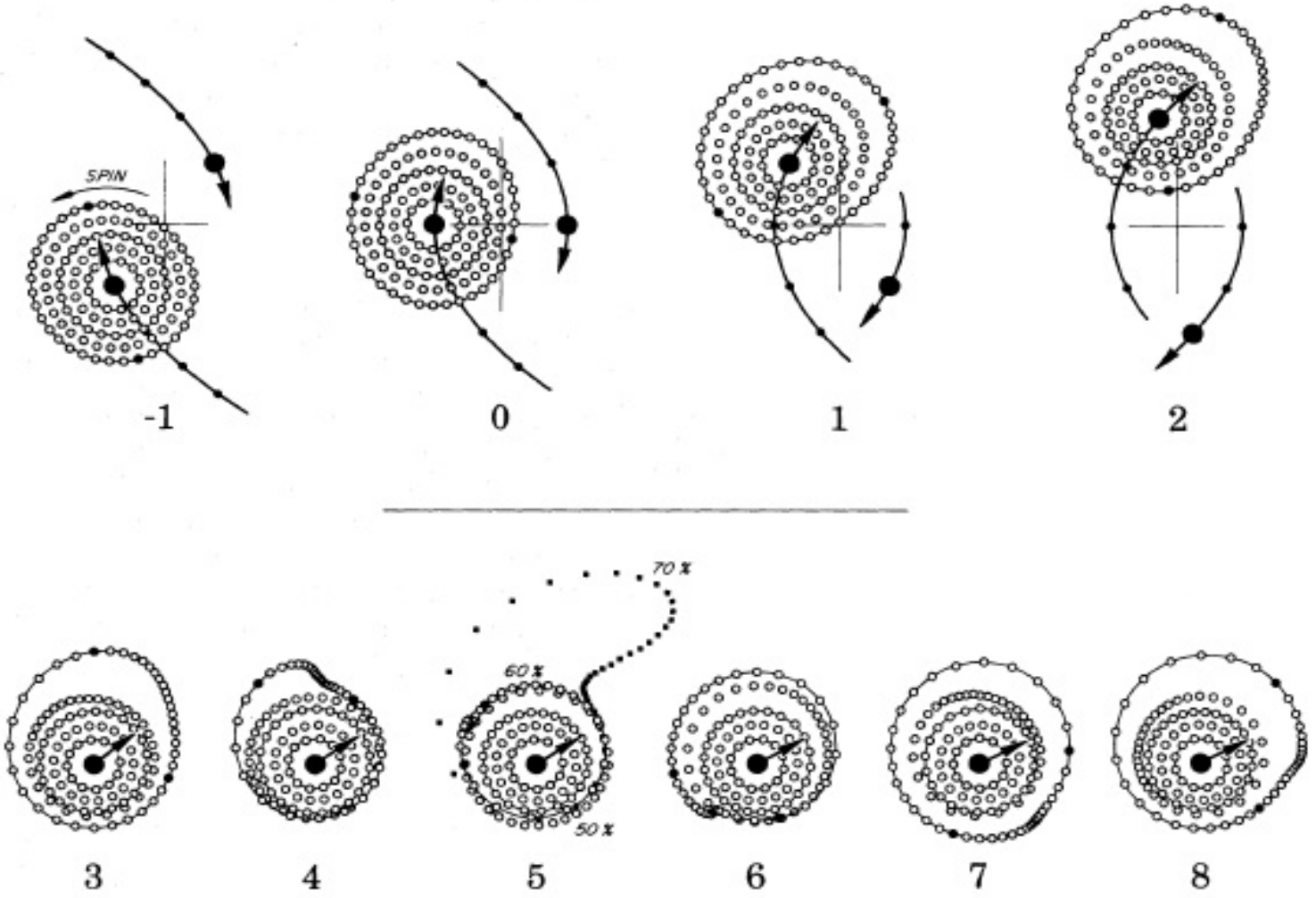

FIG. 1.—A flat retrograde ($i = 180°$) parabolic passage of a companion of equal mass. The two small filled circles denote test particles from the $0.6R_{min}$ ring which, in the absence of the encounter, would have reached positions exactly to the right and left of the victim mass at $t = 0$. The filled squares at $t = 5$ depict additional test particles from $0.7R_{min}$. (Note the partial interpenetrations of the outermost rings at $t = 4$, 5, and 6, and their continuing oscillations thereafter.)

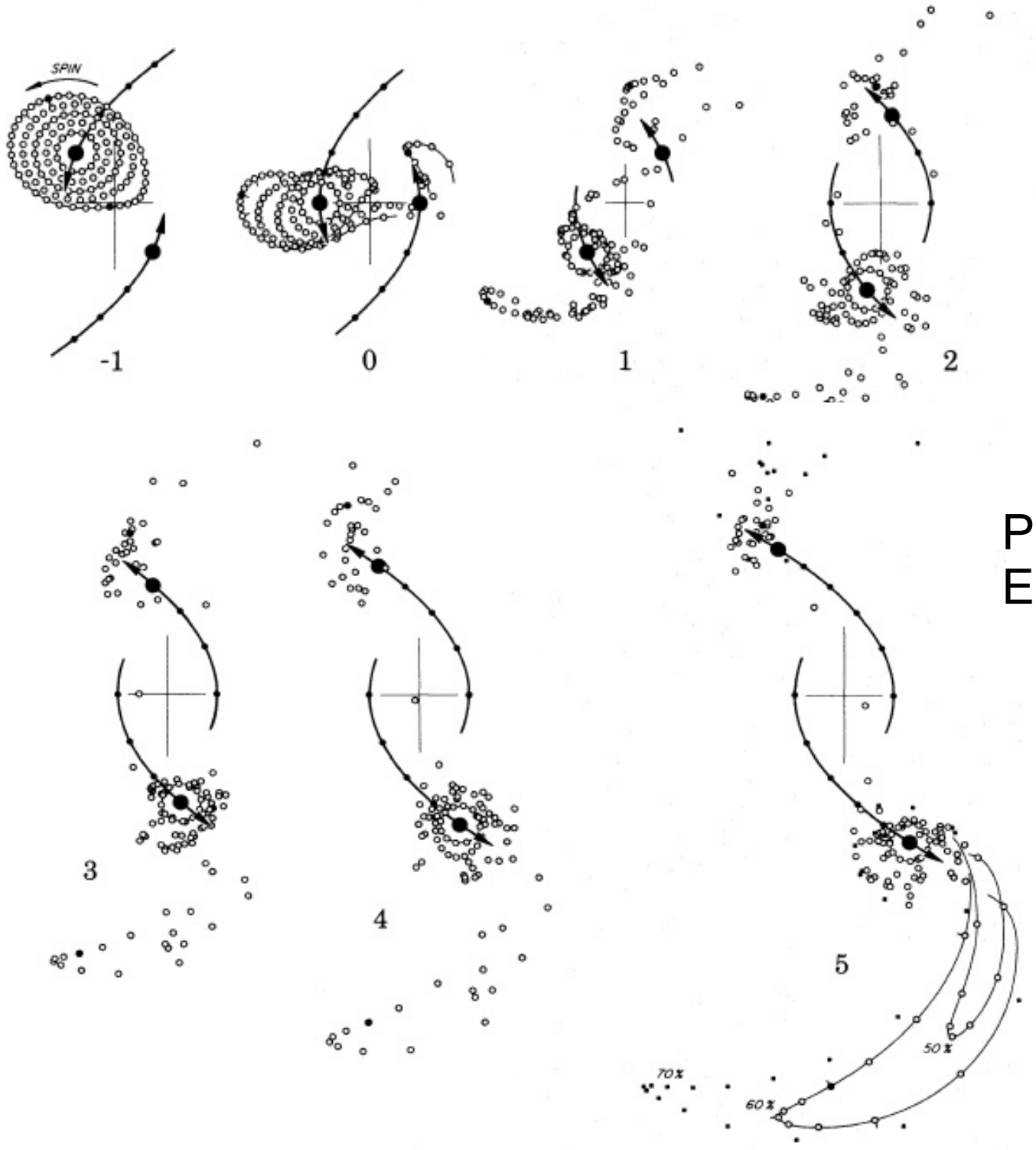

PROGRADE
ENCOUNTERS

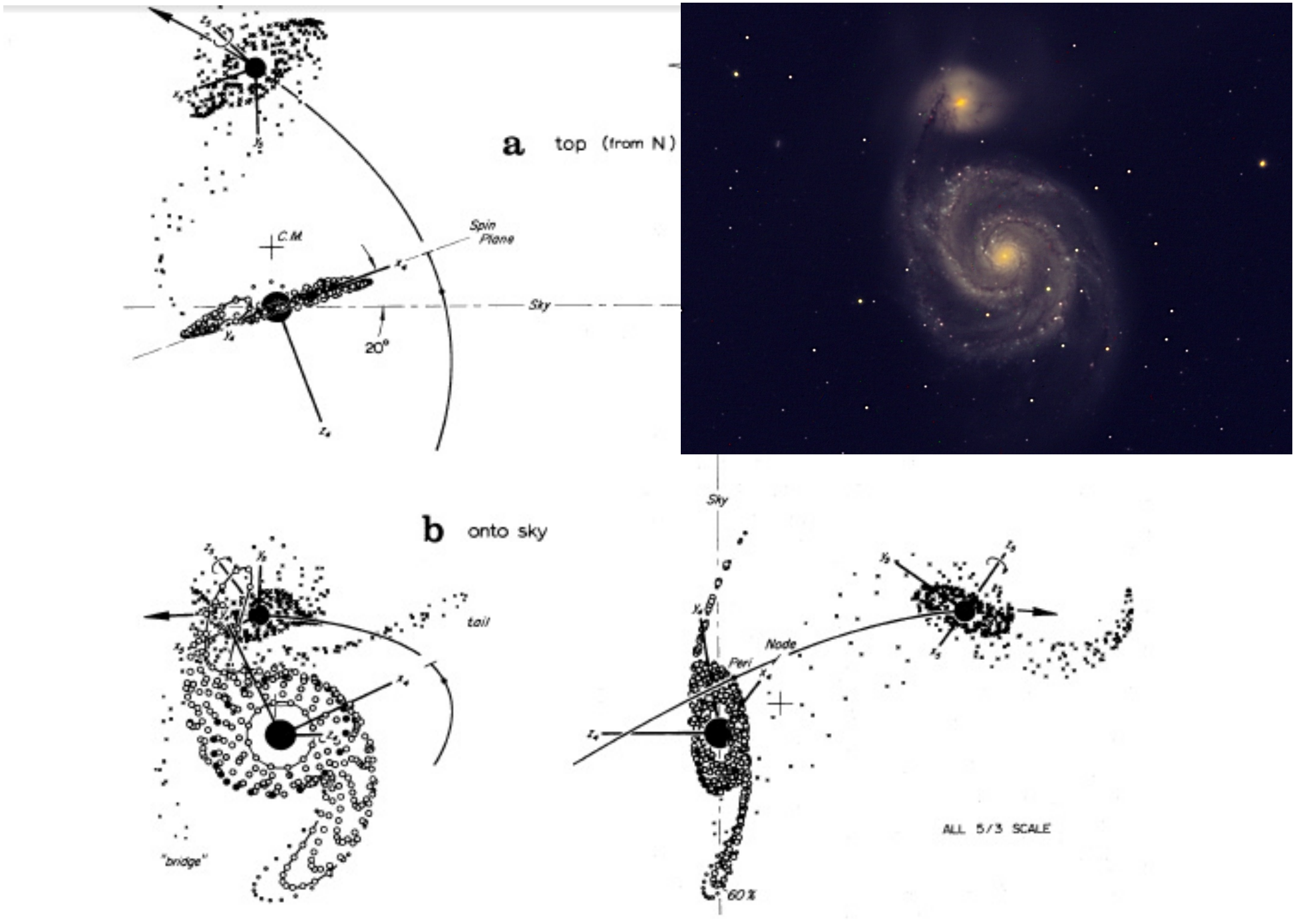

FIG. 21.—Model of the recent encounter between M51 and NGC 5195. Shown here at $t = 2.4$ are three mutually orthogonal views of the consequences of a highly elliptic $e = 0.8$ passage of a supposedly disklike "5195." This satellite was chosen to be one-third as massive, and of exactly 0.7 times the linear dimensions, of the "5194" primary—which itself contains particles from initial

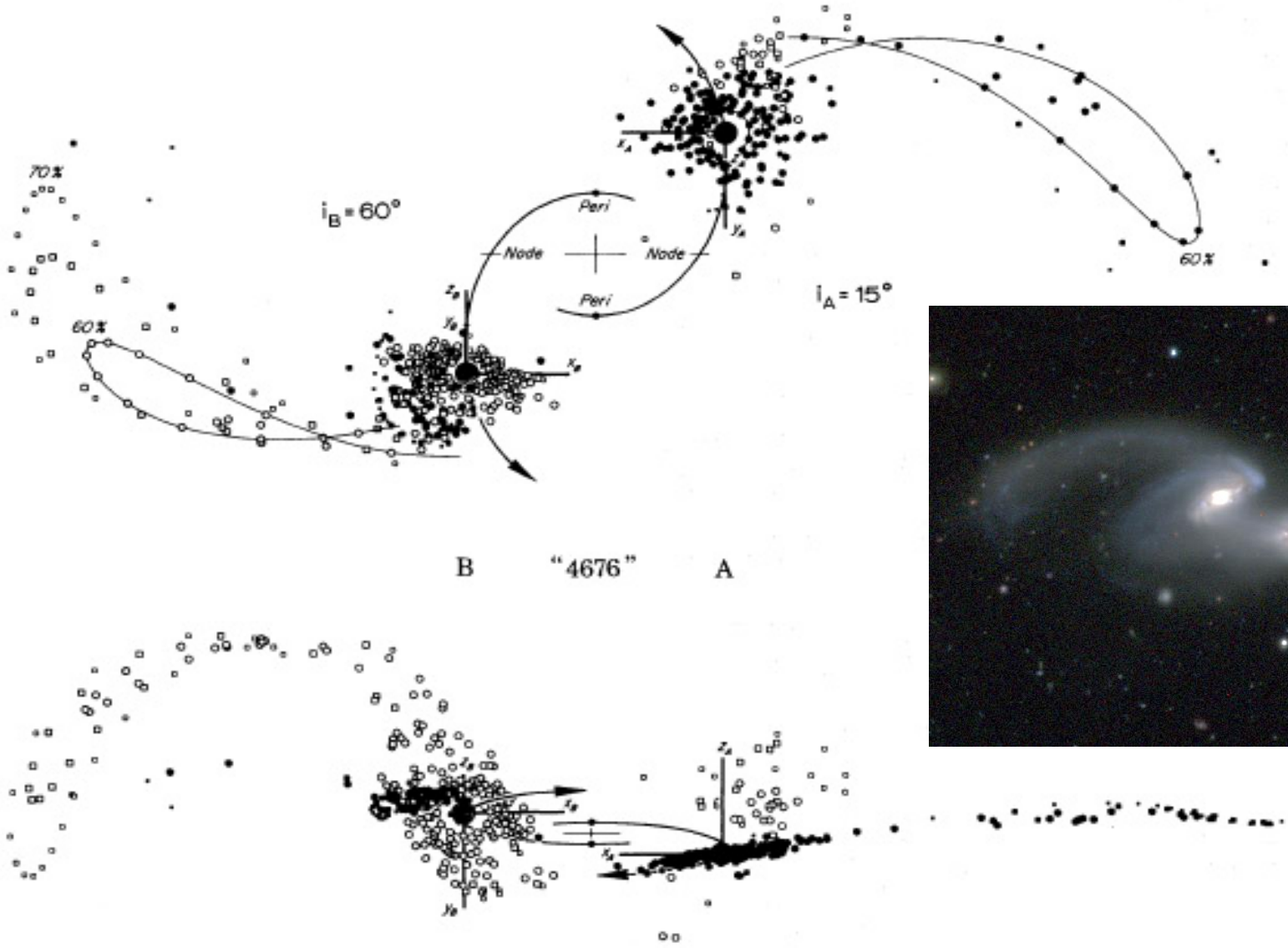

FIG. 22.—Model of NGC 4676. In this reconstruction, two equal disks of radius $0.7R_{\min}$ experienced an $e = 0.6$ elliptic encounter, having begun flat and circular at the time $t = -16.4$ of the last apocenter. As viewed from either disk, the adopted node-to-peri angles $\omega_A = \omega_B = -90°$ were identical, but the inclinations differed considerably: $i_A = 15°$, $i_B = 60°$. The resulting composite object at $t = 6.086$ (cf. fig. 18) is shown projected onto the orbit plane in the upper diagram. It is viewed nearly edge-on to the same—from $\lambda_A = 180°$, $\beta_A = 85°$ or $\lambda_B = 0°$, $\beta_B = 160°$—in the lower diagram meant to simulate our actual view of that pair of galaxies. The filled and open symbols distinguish particles originally from disks A and B, respectively.

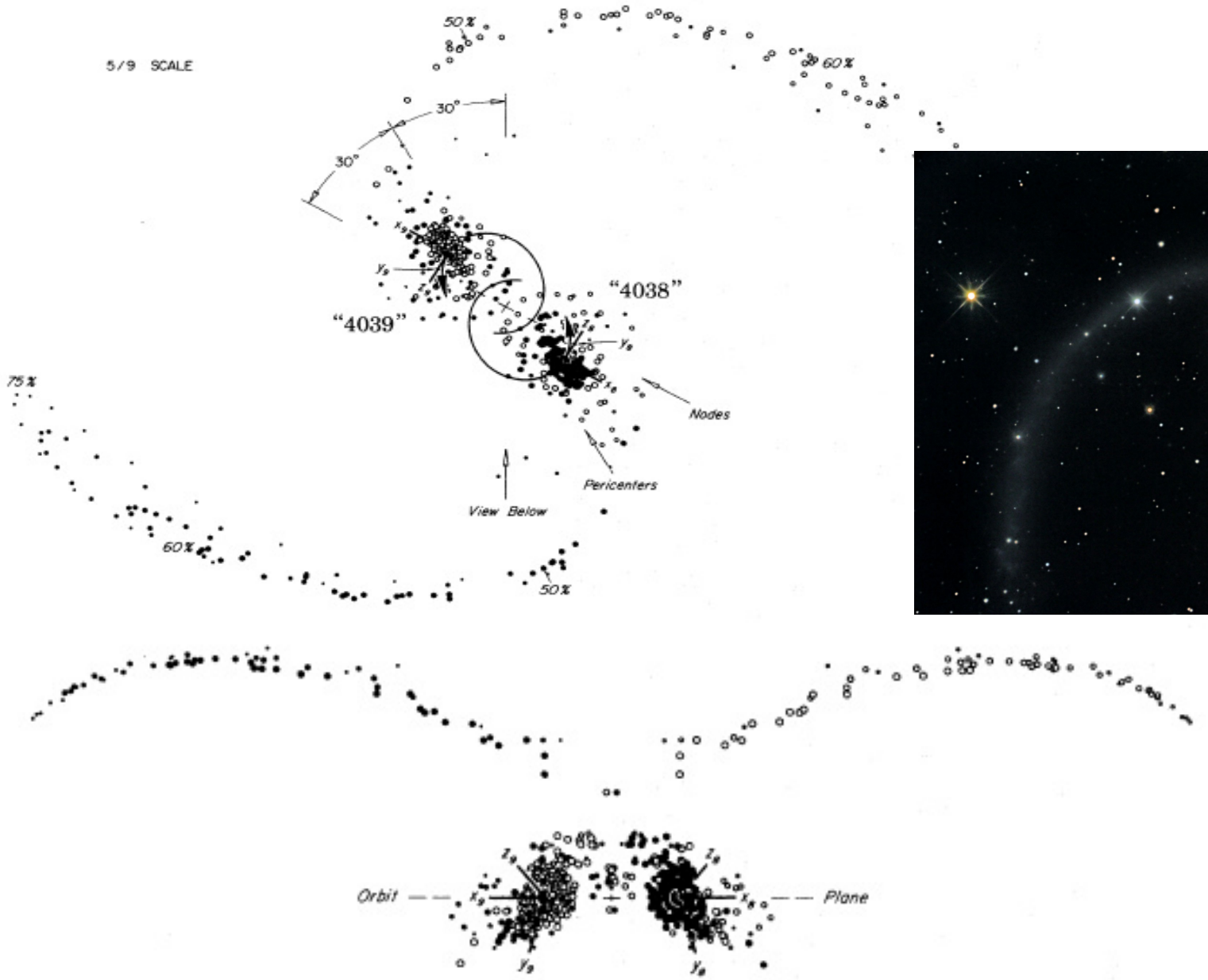

FIG. 23.—Symmetric model of NGC 4038/9. Here two identical disks of radius $0.75R_{\min}$ suffered an $e \approx 0.5$ encounter with orbit angles $i_8 = i_9 = 60°$ and $\omega_8 = \omega_9 = -30°$ that appeared the same to both. The above all-inclusive views of the debris and remnants of these disks have been drawn exactly normal and edge-on to the orbit plane; the latter viewing direction is itself 30° from the line connecting the two pericenters. The viewing time is $t = 15$, or slightly past apocenter. The filled and open symbols again disclose the original loyalties of the various test particles.

c) *Stoking the Furnace?*

We have deliberately not touched earlier on the well-known tendency (e.g., Burbidge *et al.* 1963; Zwicky 1967; Arp 1969*b*, 1971*b*; Stockton 1972) of the various tails, plumes, and intergalactic bridges to involve at least one galaxy whose own color or spectrum is often unusual, or which has a high surface brightness, or which contains oddly placed absorbing material and/or emitting regions.

That such intrinsic evidence of "strangeness" has itself contributed to the reluctance to regard the external features as tidal is both clear and understandable. Nevertheless —well short of such really exotic cases as the "jets" of M87 and 3C 273—we cannot help feeling that even this share of reluctance has been somewhat excessive: Would not the violent mechanical agitation of a close tidal encounter—let alone an actual merger—already tend to bring *deep* into a galaxy a fairly *sudden* supply of fresh fuel in the form of interstellar material, either from its own outlying disk or by accretion from its partner? And in a previously gas-poor system or nucleus, would not the relatively mundane process of prolific star formation thereupon mimic much of the "activity" that is observed?

TRANSFORMATIONS OF GALAXIES. II. GASDYNAMICS IN MERGING DISK GALAXIES

JOSHUA E. BARNES
Institute for Astronomy, University of Hawaii, 2680 Woodlawn Drive, Honolulu, HI; barnes@zeno.ifa.hawaii.edu
AND
LARS HERNQUIST[1]
Board of Studies in Astronomy and Astrophysics, U.C. Santa Cruz, Santa Cruz, CA 95064; lars@helios.ucsc.edu
Received 1995 February 27; accepted 1995 October 3

ABSTRACT

In mergers of disk galaxies, gas plays a role quite out of proportion to its relatively modest contribution to the total mass. To study this behavior, we have included gasdynamics in self-consistent simulations of collisions between equal-mass disk galaxies. The large-scale dynamics of bridge- and tail-making, orbit decay, and merging are not much altered by the inclusion of a gaseous component. However, tidal forces during encounters cause otherwise stable disks to develop bars, and the gas in such barred disks, subjected to strong gravitational torques, flows toward the central regions where it may fuel the kiloparsec-scale starbursts seen in some interacting disk systems. Similar torques on the gas during the final stages of a collision yield massive gas concentrations in the cores of merger remnants, which may be plausibly identified with the molecular complexes seen in objects such as NGC 520 and Arp 220. This result appears insensitive to the detailed microphysics of the gas, provided that radiative cooling is permitted. The inflowing gas can dramatically alter the *stellar* morphology of a merger remnant, apparently by deepening the potential well and thereby changing the boundaries between the major orbital families.

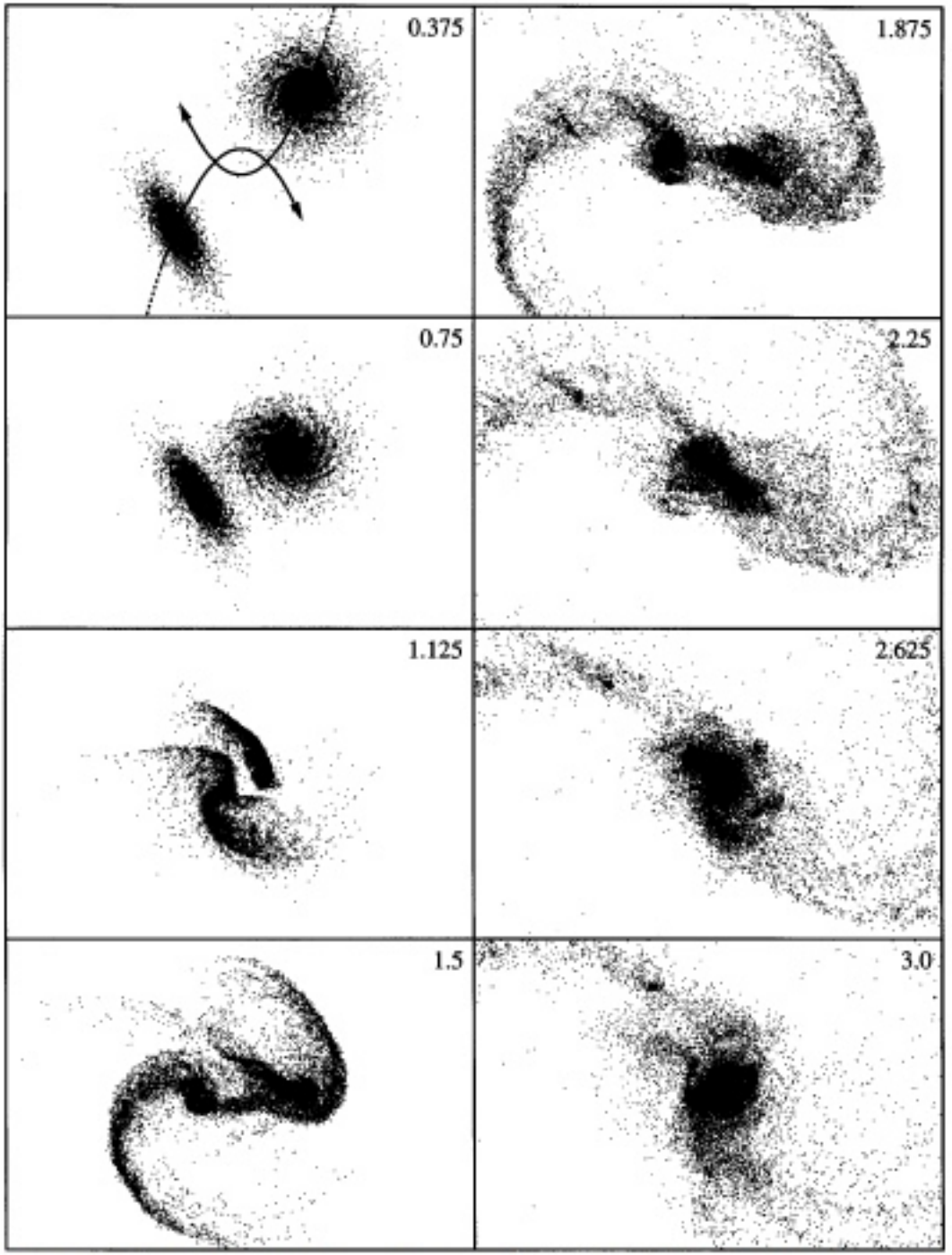

FIG. 4.—Evolution of the stellar distribution in encounter A, projected onto the orbital plane. The scale is the same as in Fig. 3.

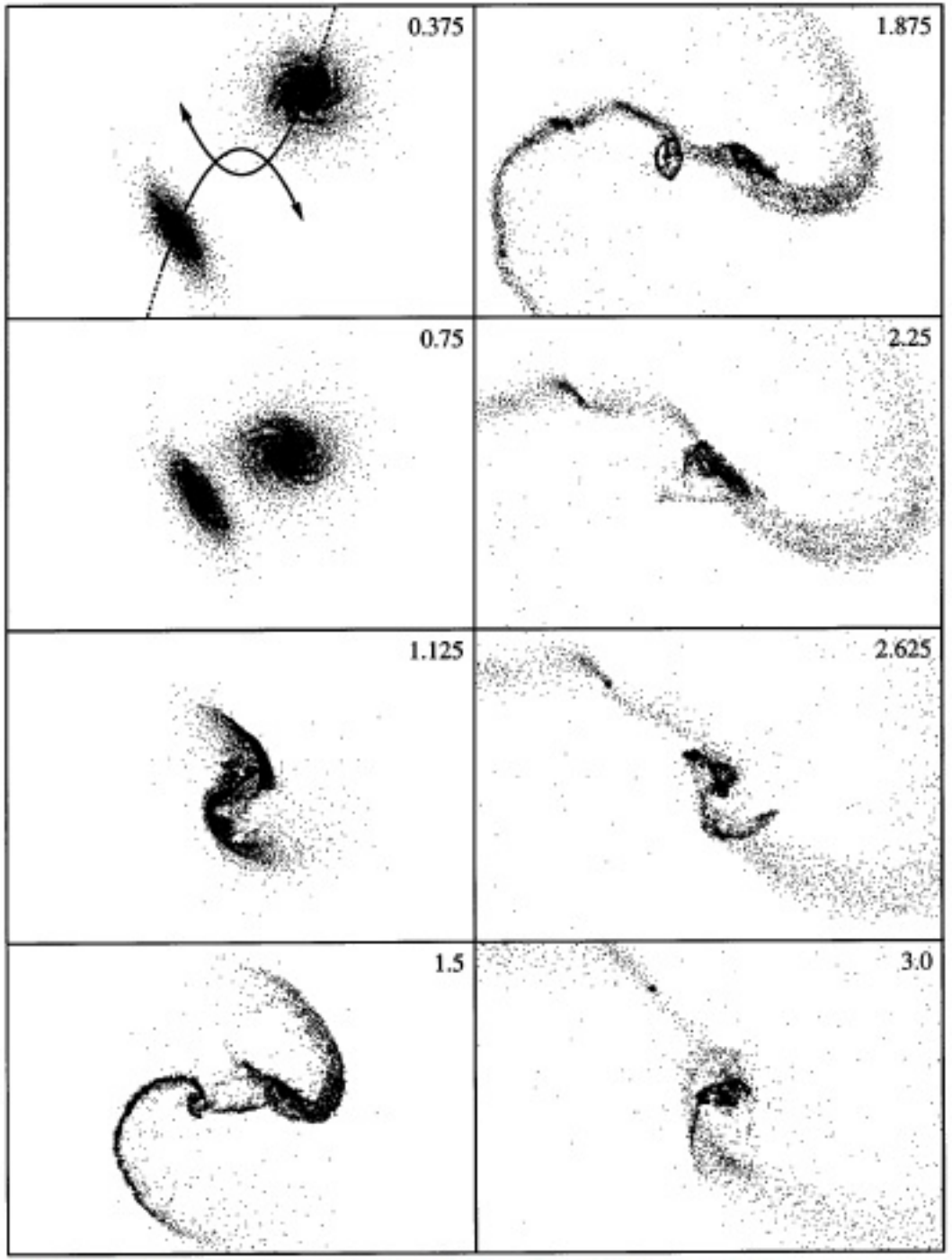

FIG. 3.—Evolution of the gas distribution in encounter A, projected onto the orbital plane. These frames are 3.6 × 2.4 length units; elapsed time is shown t the upper right of each. The first frame also shows the projected parabolic orbits of the infalling galaxies.

Remnants of simulations of the merger of two equal mass galaxies

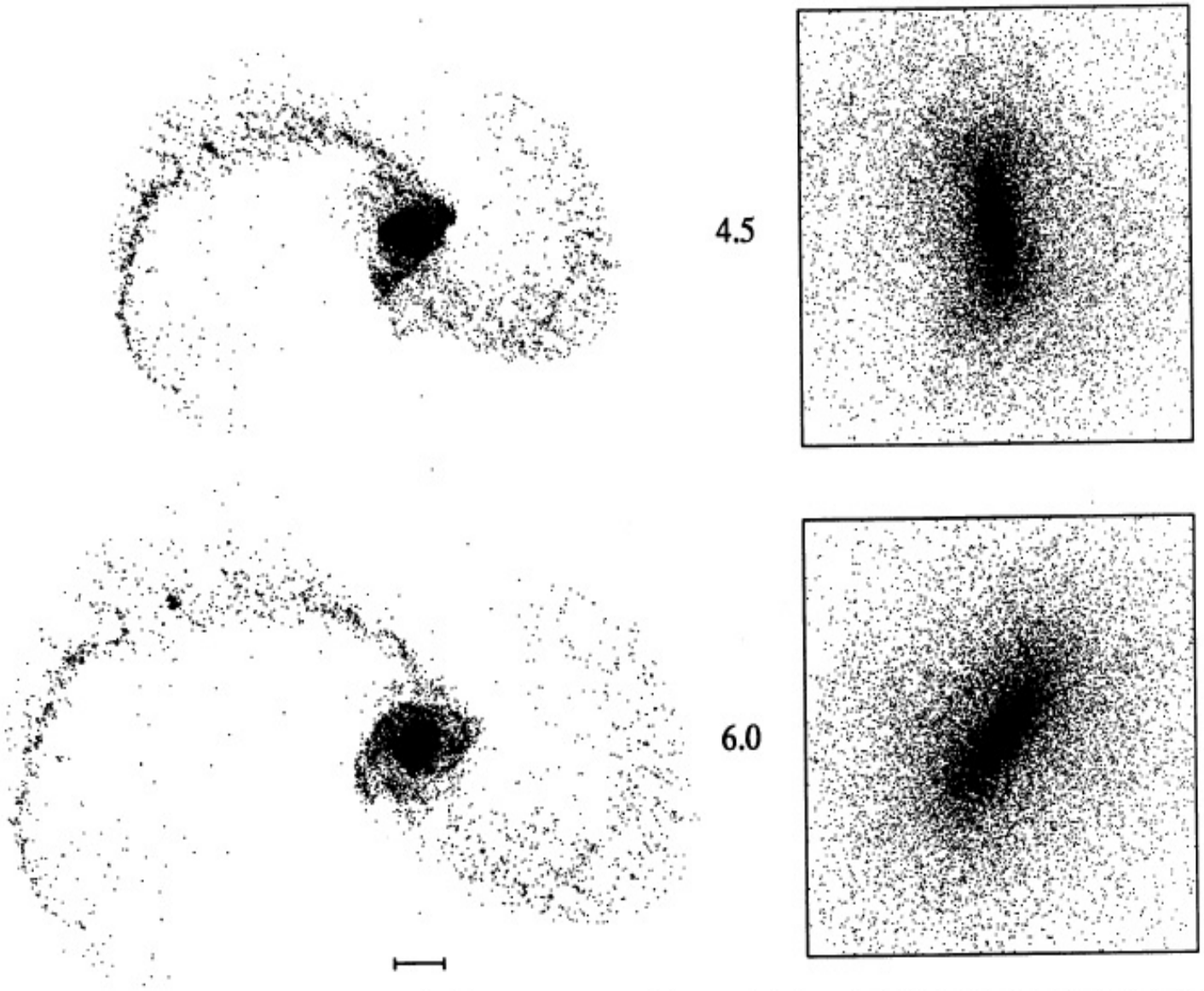

FIG. 11.—Large-scale (*left*) and small-scale (*right*) structure of the merger remnant in encounter **A**, projected onto the orbital plane, at times 3, 4.5, and 6. The boxes, enlarged by a factor of 10 from their unframed counterparts, are 0.8 × 0.8 length units. Again, only 50% of the bulge particles are plotted.

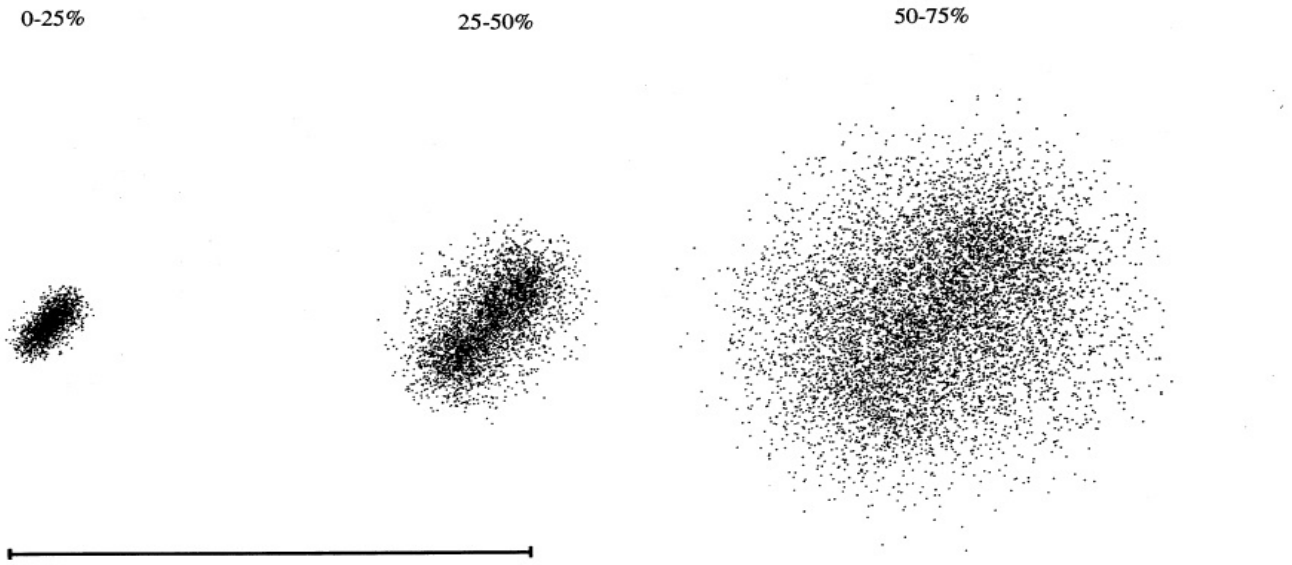

FIG. 15.—Luminous particles from the remnant produced by encounter **A** at time $t = 6$, binned by their specific binding energy. On the left is the 0%–25% bin, thinned by a factor of 4 to reduce crowding. In the middle is the 25%–50% bin, thinned by a factor of 2. On the right is the 50%

Original profile

After merging

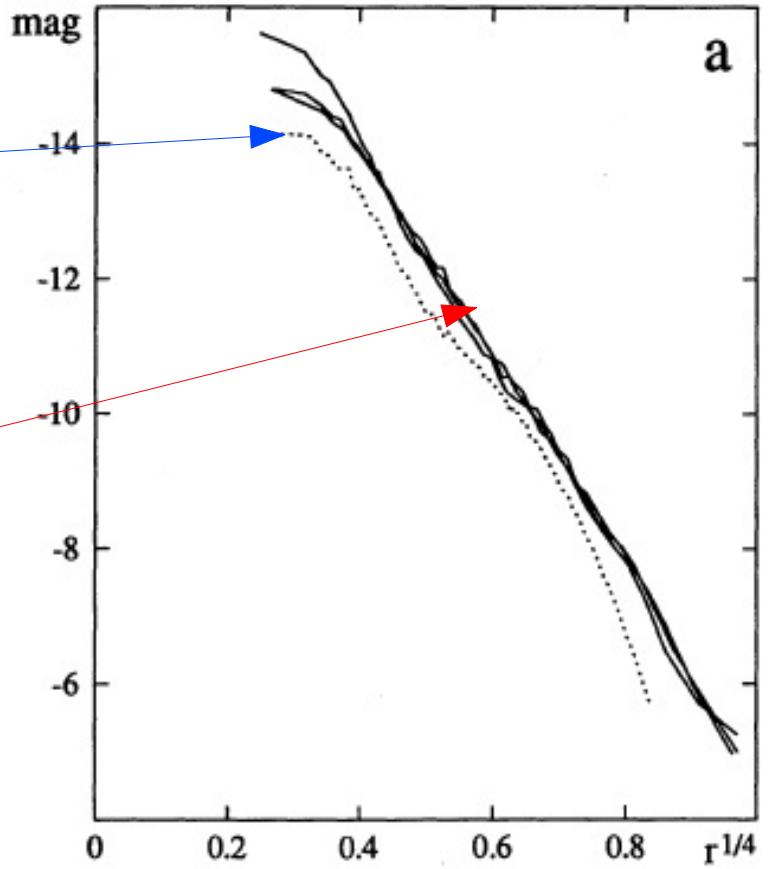

Major mergers with gas

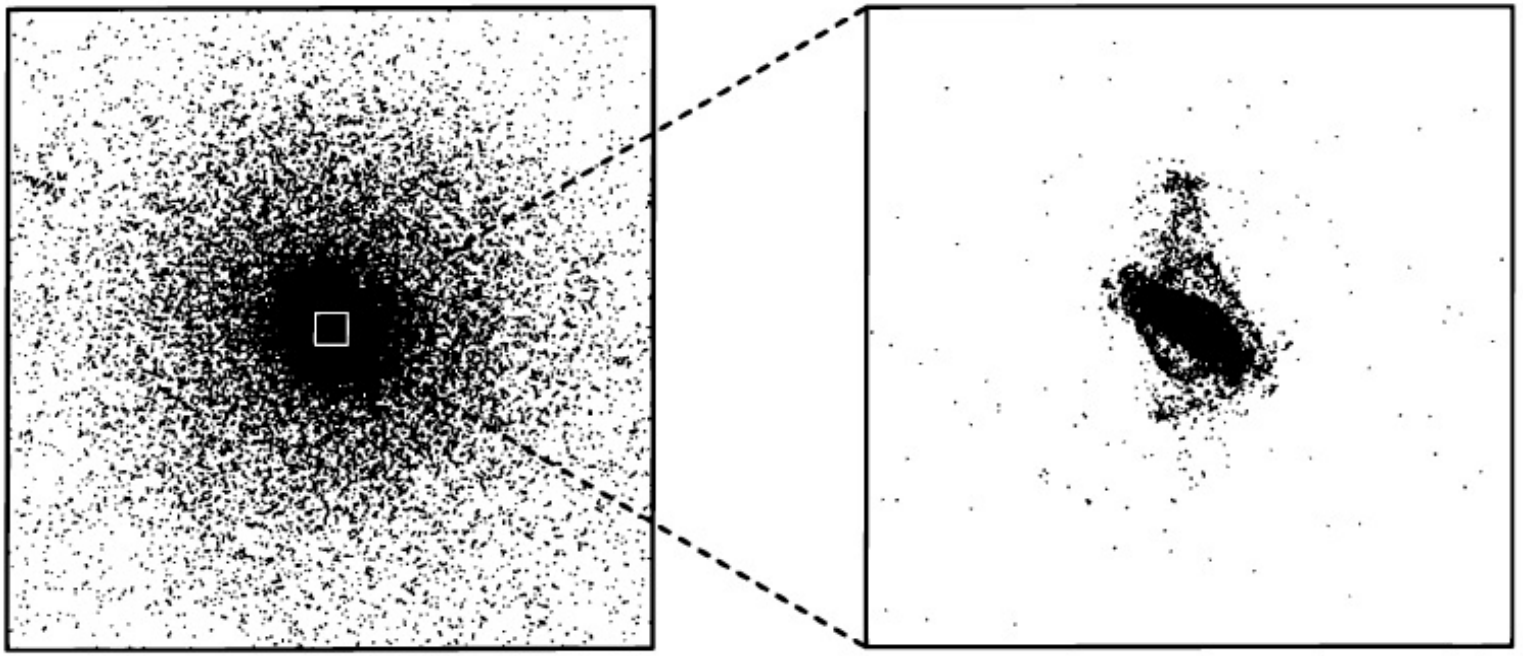

FIG. 14.—Views of stars (*left*) and gas (*right*) in the merger remnant produced by encounter A at time $t = 6$. The stellar view is 0.8×0.8 length units, while the view of the gas is enlarged by a factor of 20. Over 60% of all the gas in this remnant lies in this dense central blob.

Formation of elliptical galaxies in a cosmological context

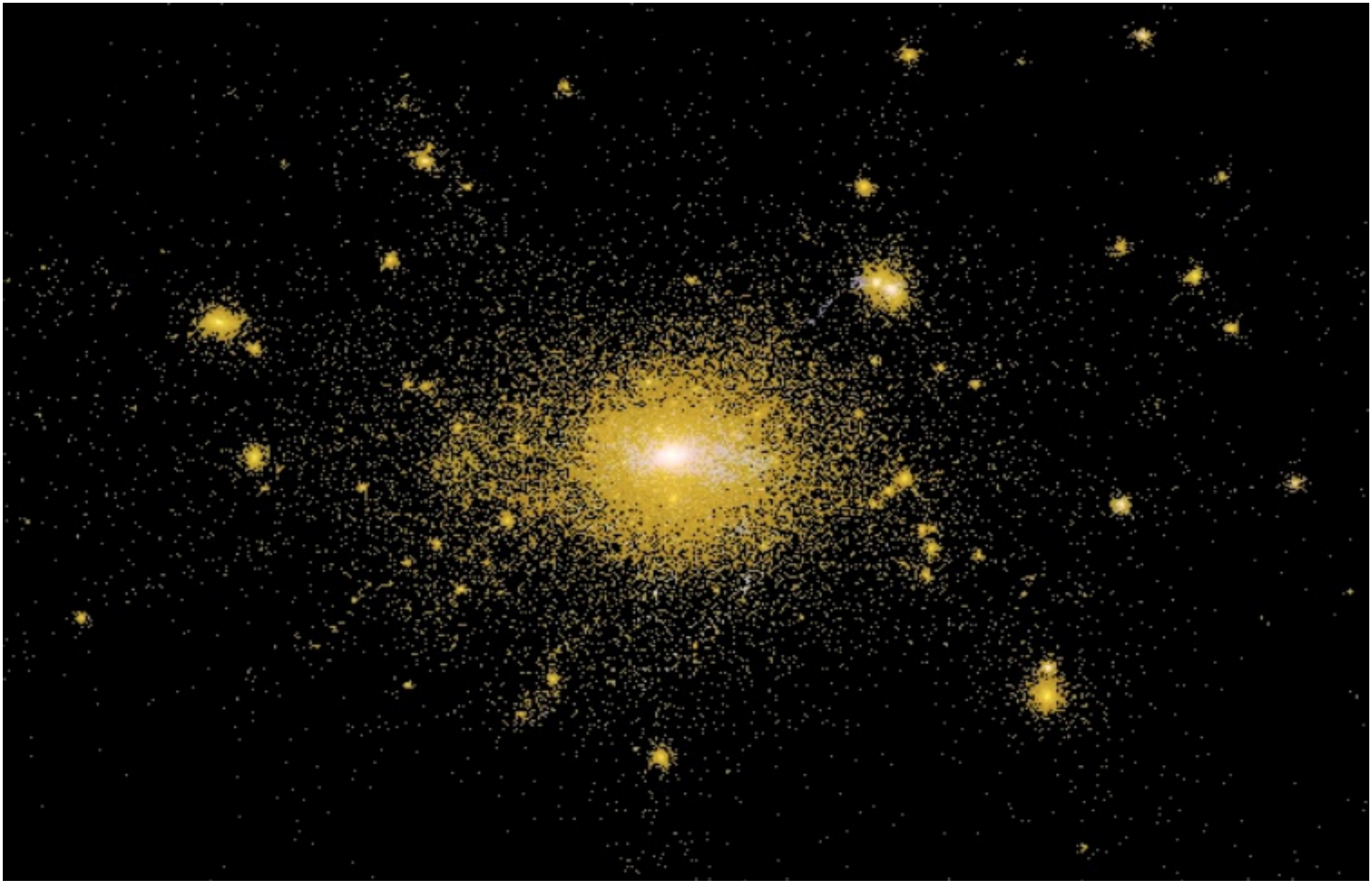

Two-phase model

Location where stars form as a function of age

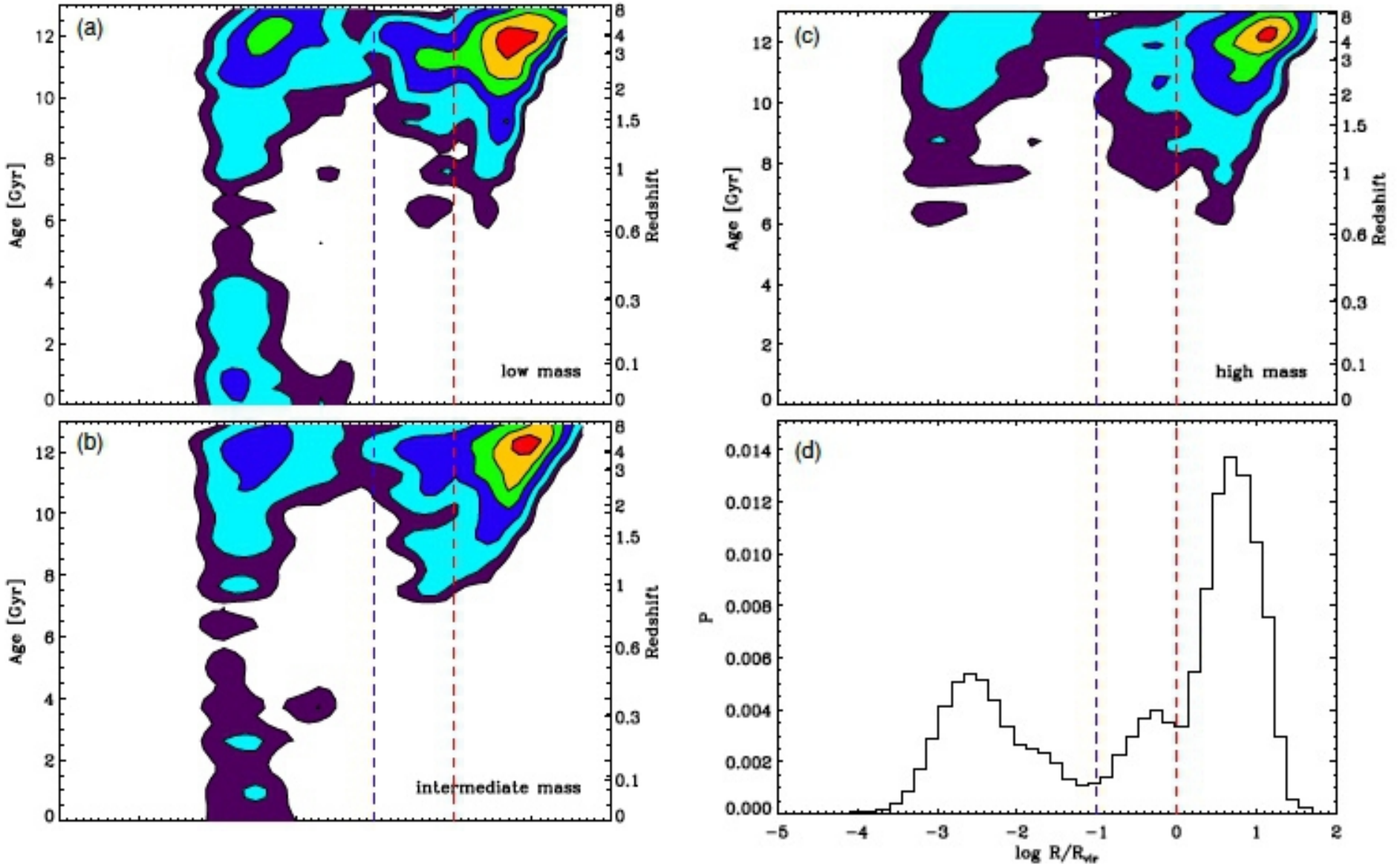

log R/R_{vir}

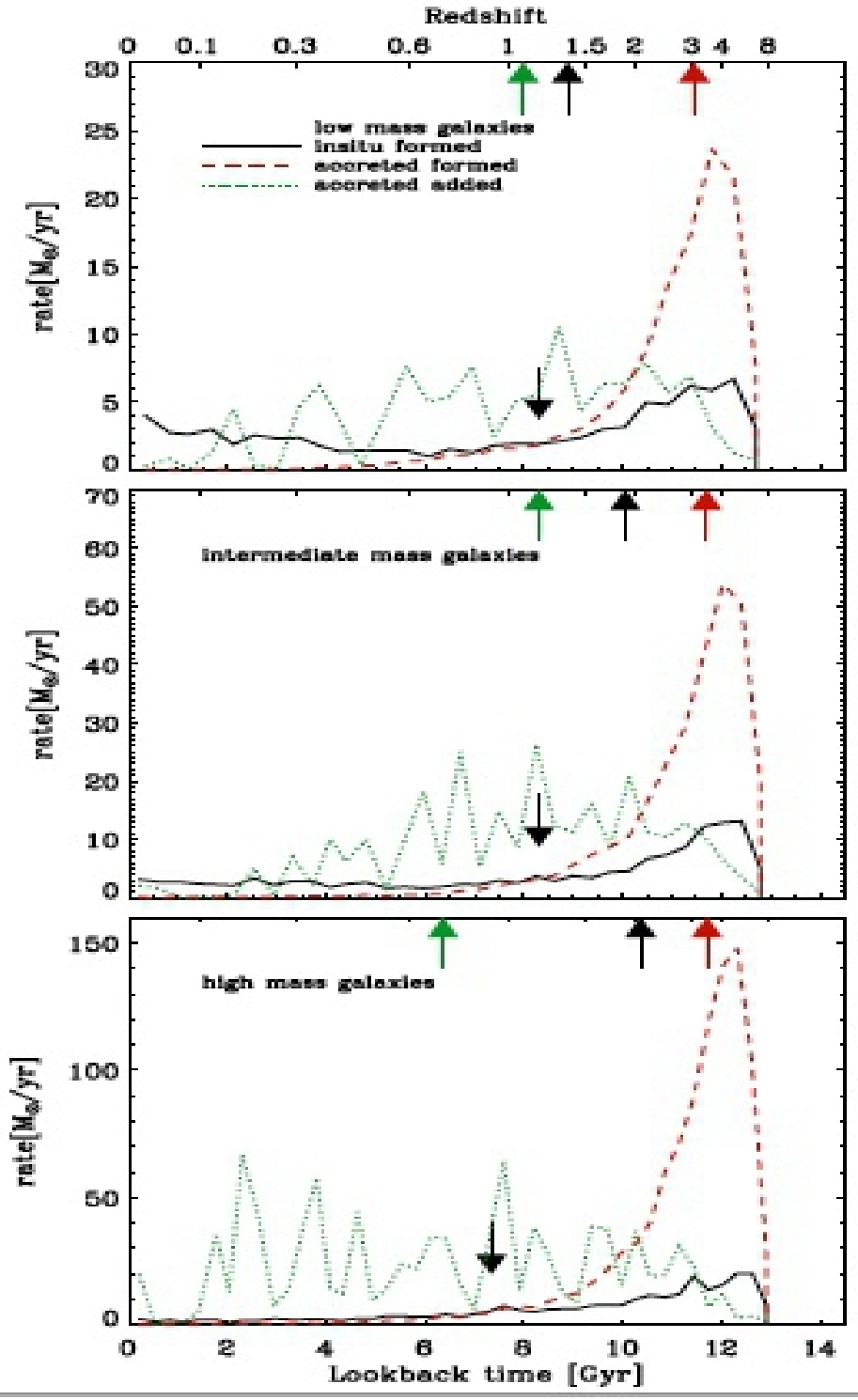

"In situ formed":
stars formed from cooling gas in central galaxy

"In situ accreted formed":
star formed from gas accreted by central galaxy in merging satellites.

"Accreted added":
stars added by merging satellites

Size-mass relation at different redshifts

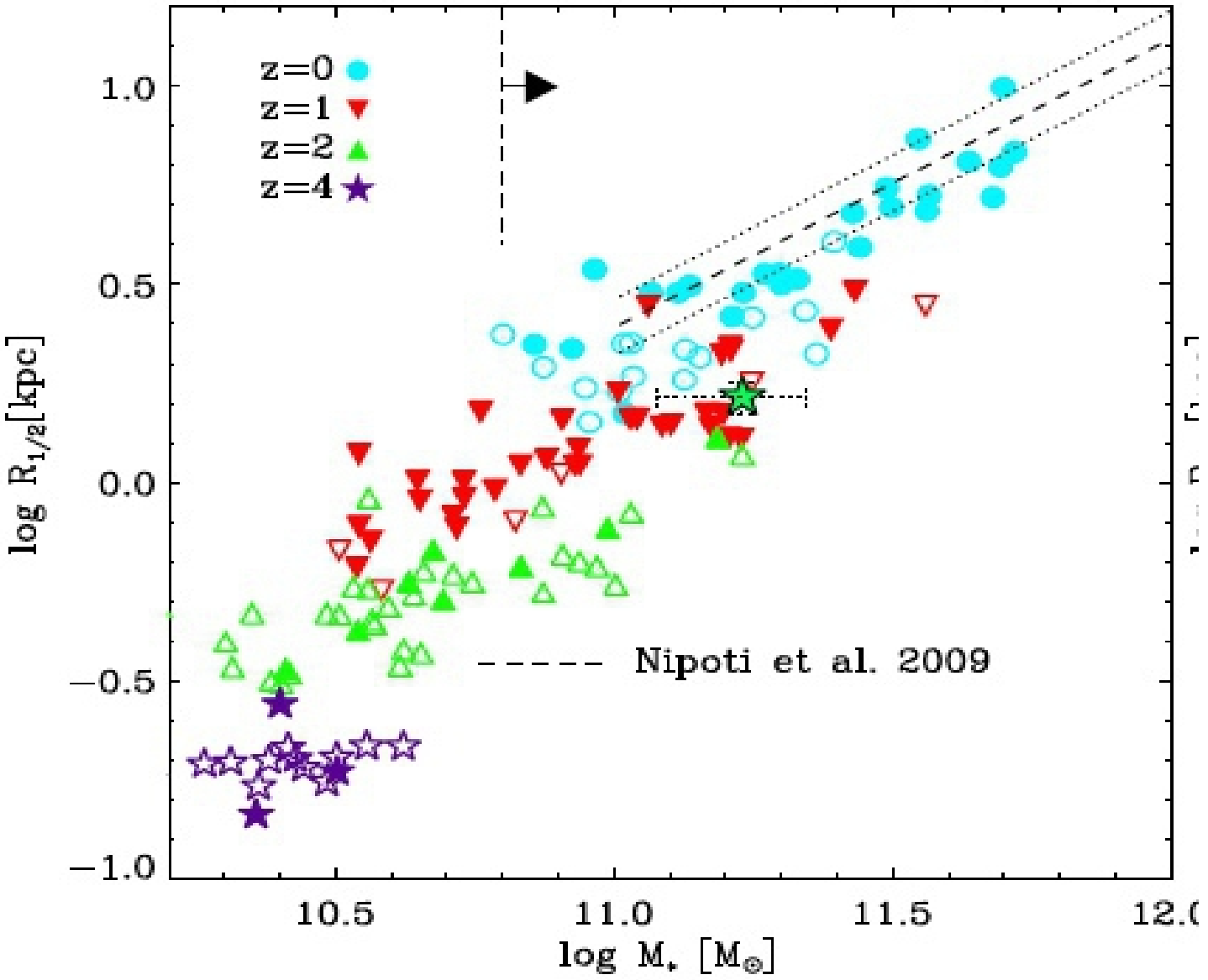

Velocity dispersion-mass relation

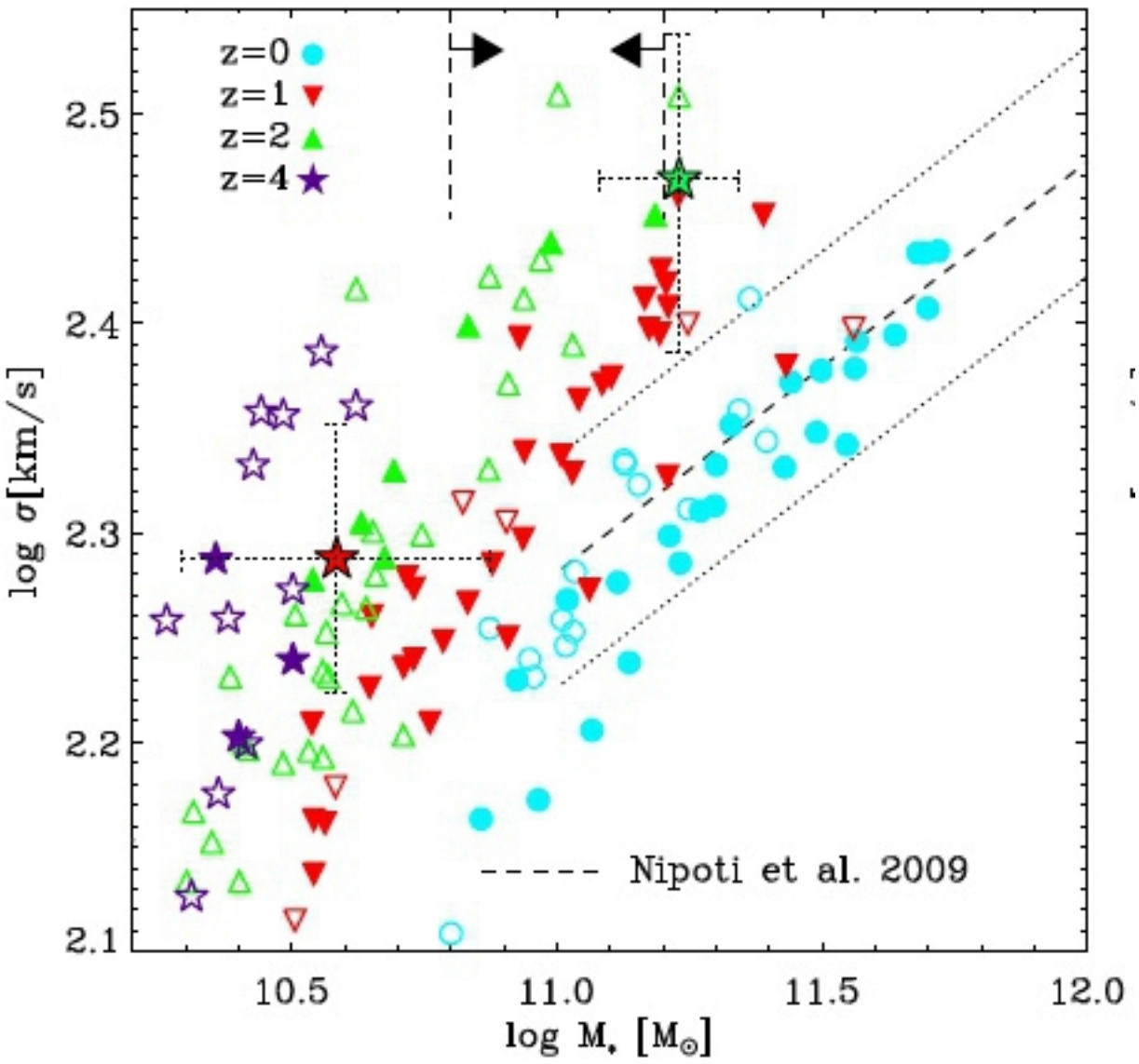

A CLOSER LOOK AT THE ACCRETED COMPONENTS

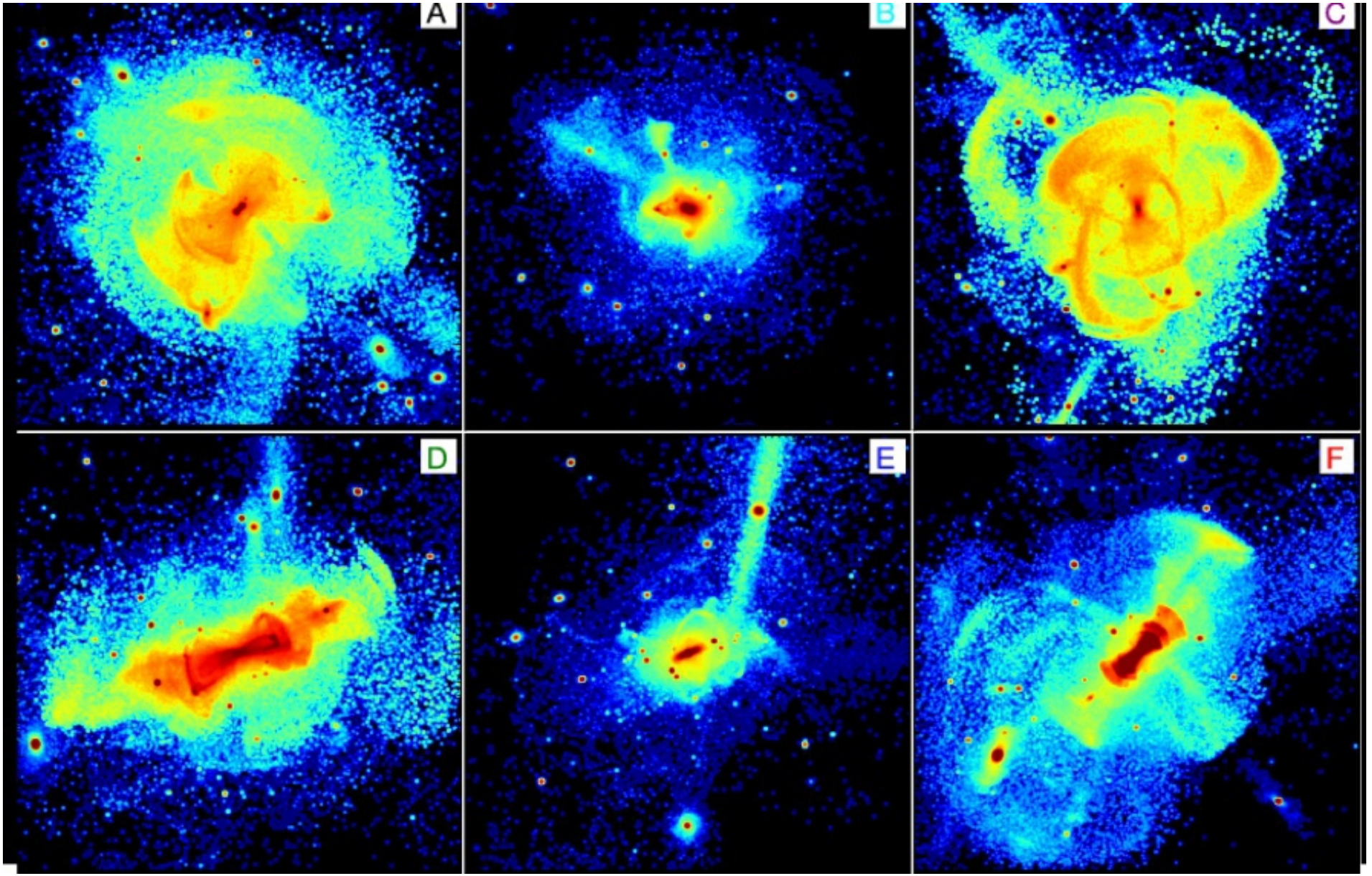

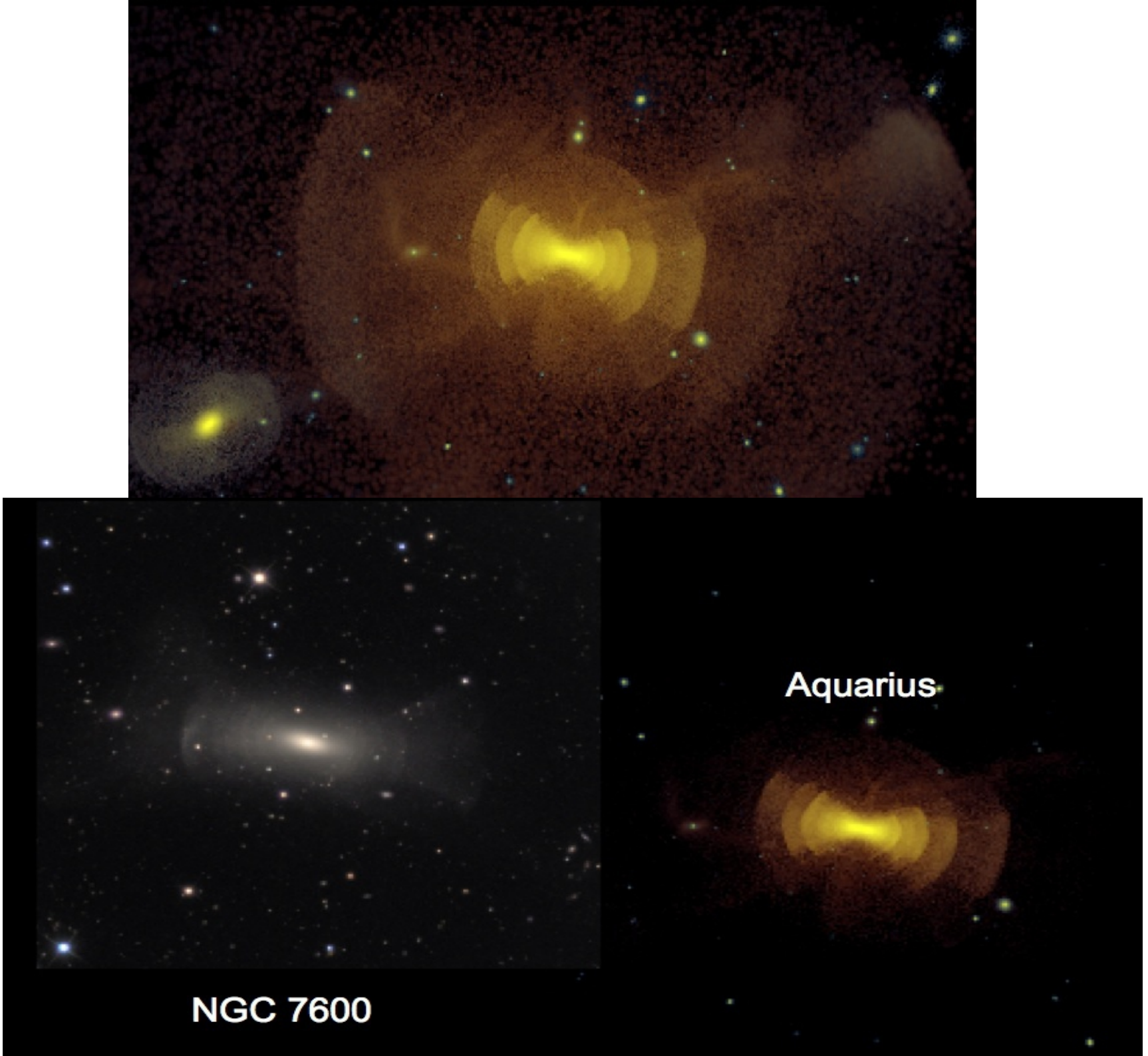
Aquarius
NGC 7600

THE POPULATION OF SPIRAL GALAXIES

Disk Galaxies: Observational Facts

Exponential Surface Brightness Profiles

- Disk galaxies have surface brightness profiles that often are close to exponential.
- Deviations from exponential at small radii are attributed to bulge and/or bar.
- Deviations from exponential at large radii are attributed to star formation thresholds, radial migration, and/or maximum angular momentum...

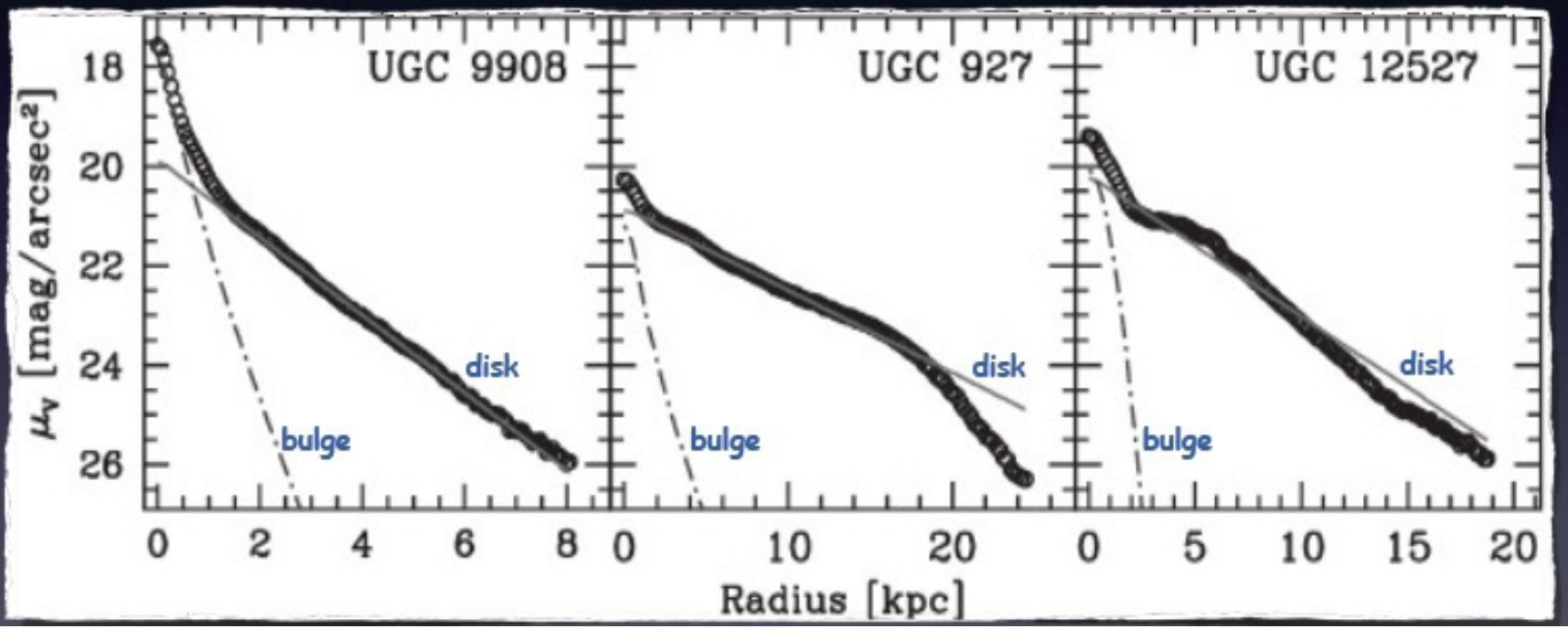

Disk Galaxies: Observational Facts

Flat Rotation Curves

Disk galaxies have flat rotation curves. Unfortunately, it is difficult to obtain unique disk-halo(-bulge) decompositions....

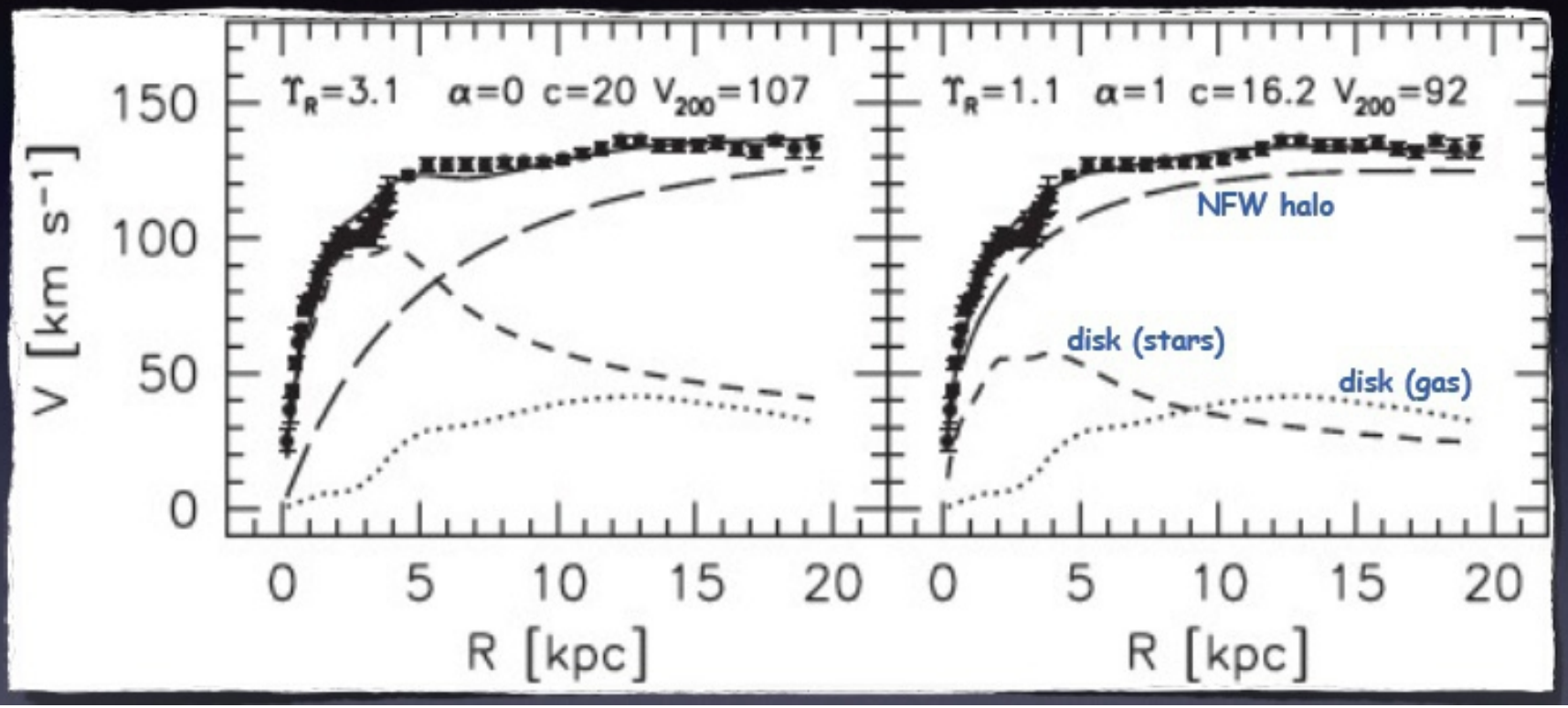

Disk Galaxies: Observational Facts

Scaling Relations

Brighter disks

- are larger
- are redder
- have higher central SB
- have smaller gas mass fractions
- rotate faster (Tully-Fisher relation)

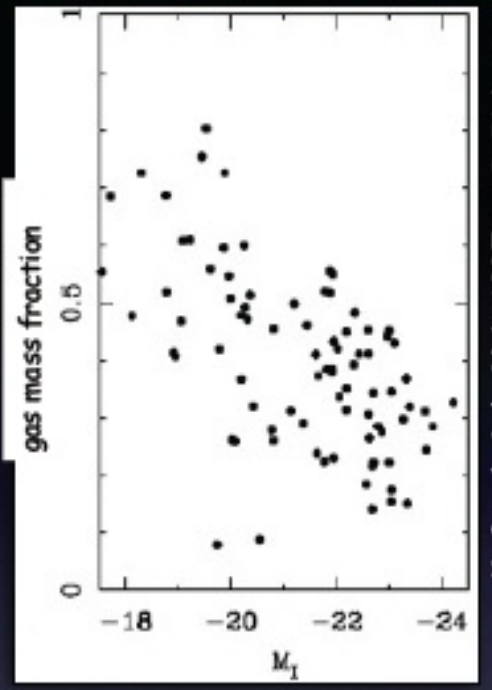

McGaugh & de Blok, 1997, ApJ, 534, 146

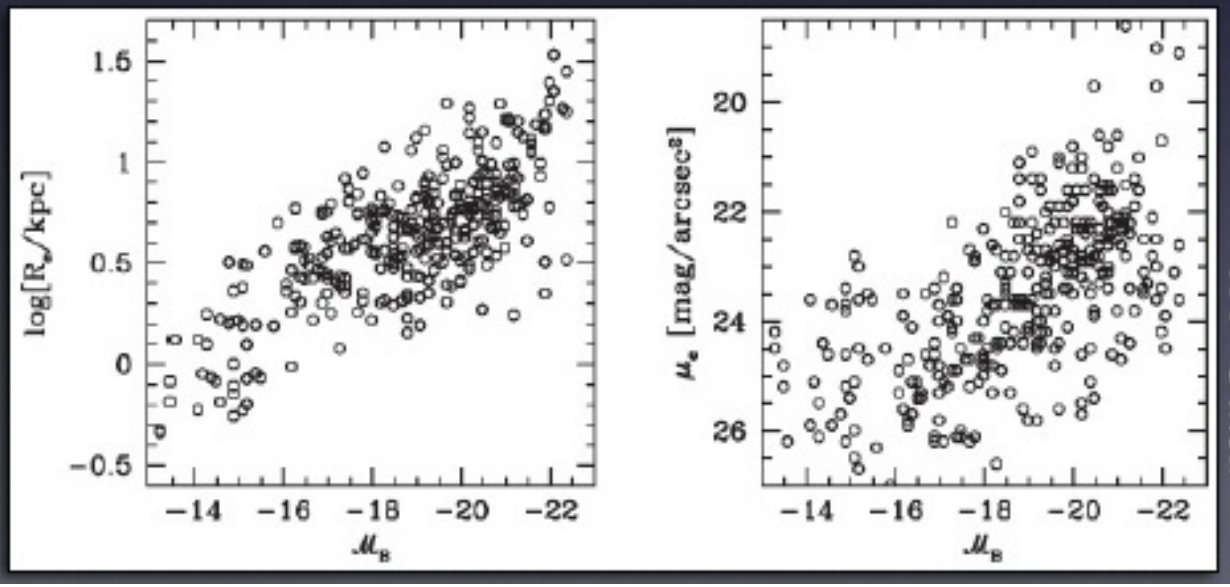

MBW, Fig. 2.20

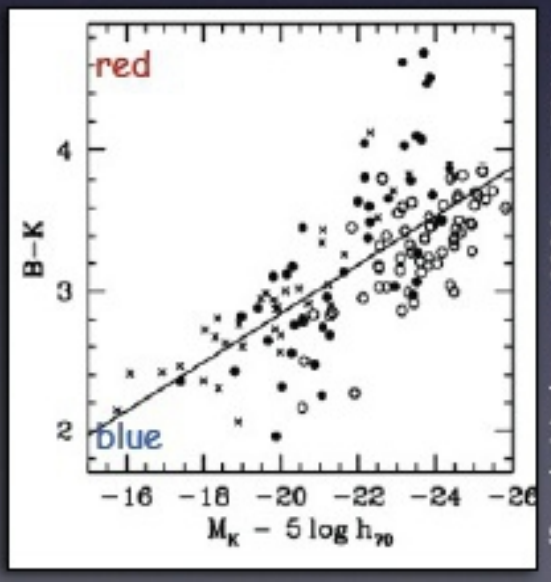

vdBosch & Dalcanton, 2000, ApJ, 534, 146

Tully-Fisher Relation in different Photometric Bands

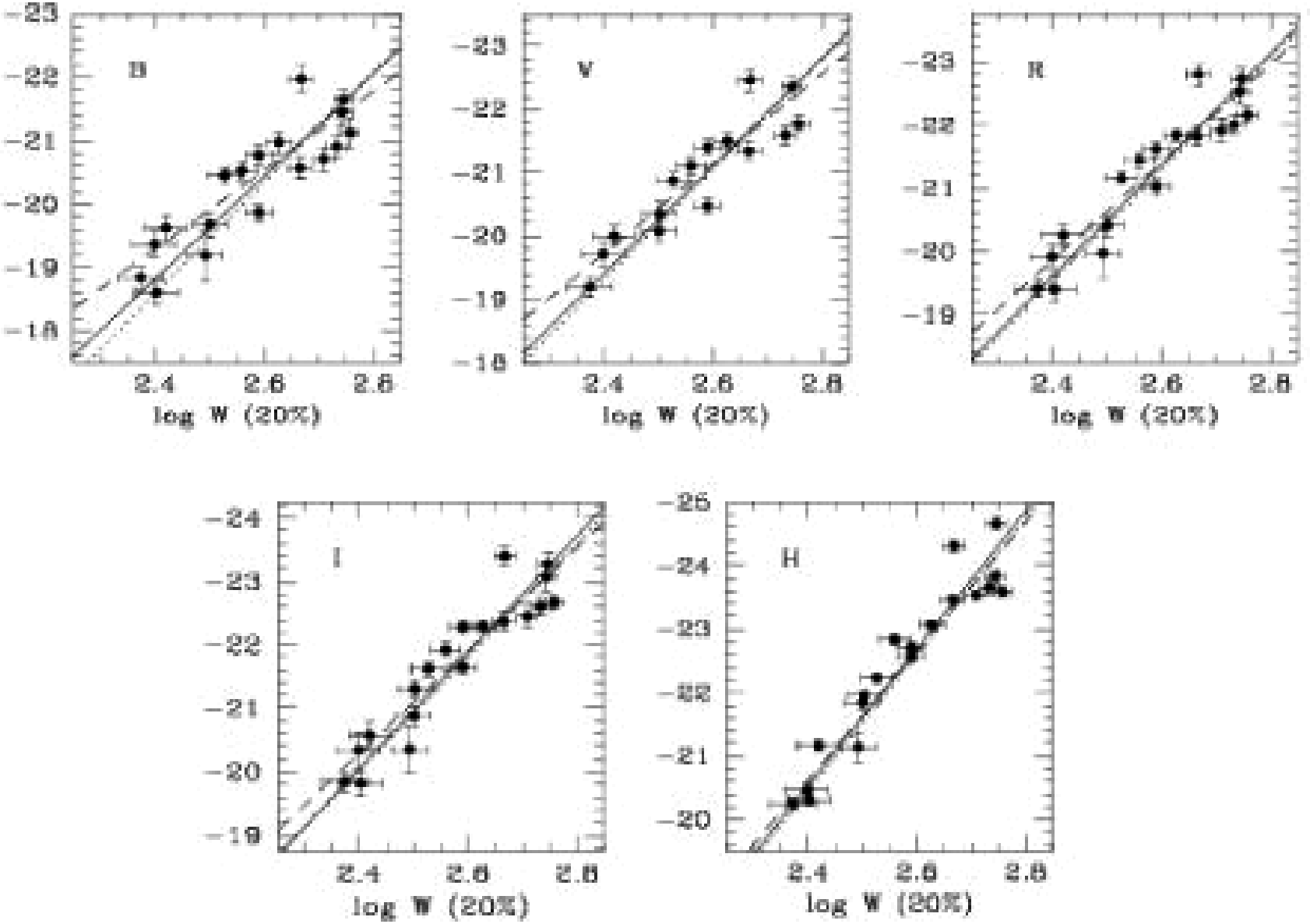

Stellar mass as a function of circular velocity

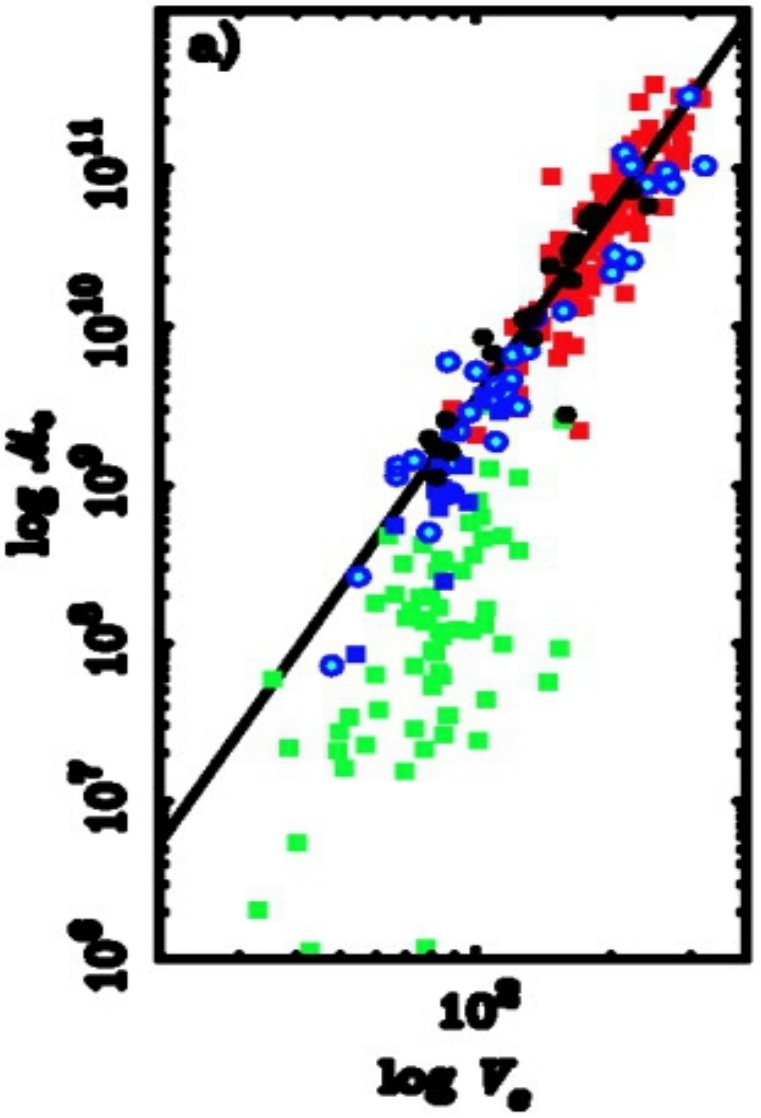

Stellar + gas (baryonic) mass as a function of circular velocity

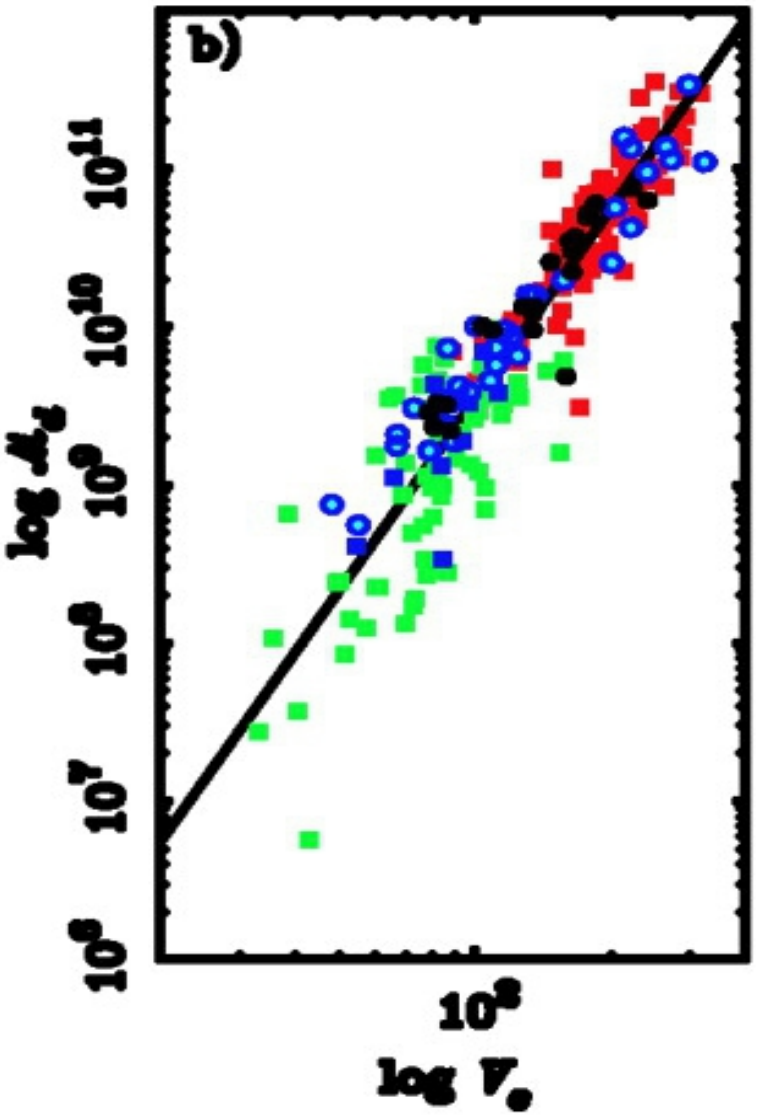

The Formation of Disk Galaxies

Hot (shock-heated) gas inside extended dark matter halo cools radiatively,

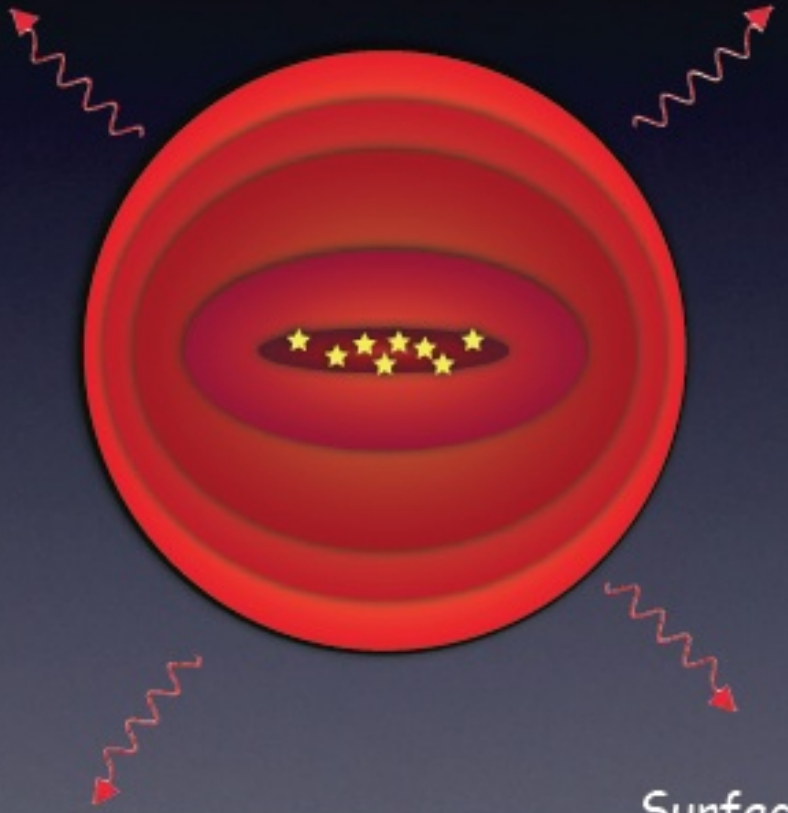

As gas cools, its pressure decreases causing the gas to contract

Since emission of photons is isotropic, angular momentum of cooling gas is conserved.

As gas sphere contracts, it spins up, and flattens

Surface density of disk increases, `triggering' star formation; a disk galaxy is born...

Simple Model to Predict Disk Sizes and Rotation Curves From Dark Halo Properties plus assumption that Gas Conserves Angular Momentum

For a singular isothermal sphere the density profile is just

$$\rho(r) = \frac{V_c^2}{4\pi G r^2}, \qquad (1)$$

we define the limiting radius of a dark halo to be the radius r_{200} within which the mean mass density is $200\rho_{crit}$, where ρ_{crit} is the critical density for closure at the redshift z when the halo is identified. Thus, the radius and mass of a halo of circular velocity V_c seen at redshift z are

$$r_{200} = \frac{V_c}{10H(z)}; \quad M = \frac{V_c^2 r_{200}}{G} = \frac{V_c^3}{10GH(z)}, \qquad (2)$$

where

$$H(z) = H_0\left[\Omega_{\Lambda,0} + (1 - \Omega_{\Lambda,0} - \Omega_0)(1+z)^2 + \Omega_0(1+z)^3\right]^{1/2} \qquad (3)$$

is the Hubble constant at redshift z.

[recall $\rho_{crit} = 3\,H^2(z)/\,8\pi\,G$]

We assume that the mass which settles into the disc is a fixed fraction m_d of the halo mass. The disc mass is then

$$M_d = \frac{m_d V_c^3}{10GH(z)} \approx 1.7\times 10^{11} h^{-1}\,\mathrm{M}_\odot \left(\frac{m_d}{0.05}\right)\left(\frac{V_c}{250\,\mathrm{km\,s^{-1}}}\right)^3 \left[\frac{H(z)}{H_0}\right]^{-1}.$$

Let us **assume** an exponential profile for the disk:

$$\Sigma(R) = \Sigma_0 \exp\left(-R/R_d\right). \tag{5}$$

Here R_d and Σ_0 are the disc scalelength and central surface density, and are related to the disc mass through

$$M_d = 2\pi\Sigma_0 R_d^2. \tag{6}$$

If the gravitational effect of the disc is neglected, its rotation curve is flat at the level V_c and its angular momentum is just

$$J_d = 2\pi \int V_c \Sigma(R) R^2 \mathrm{d}R = 4\pi\Sigma_0 V_c R_d^3 = 2M_d R_d V_c. \tag{7}$$

We assume this angular momentum to be a fraction j_d of that of the halo, i.e.

$$J_d = j_d J, \tag{8}$$

and we relate J to the spin parameter λ of the halo through the definition

$$\lambda = J|E|^{1/2} G^{-1} M^{-5/2}, \tag{9}$$

where E is the total energy of the halo. Equations (7) and (8) then imply that

$$R_d = \frac{\lambda G M^{3/2}}{2V_c|E|^{1/2}}\left(\frac{j_d}{m_d}\right). \tag{10}$$

The total energy of a truncated singular isothermal sphere is easily obtained from the virial theorem by assuming all particles to be on circular orbits:

$$E = -\frac{GM^2}{2r_{200}} = -\frac{MV_c^2}{2}. \tag{11}$$

On inserting this into equation (10) and using equations (2) and (6) we get

$$R_d = \frac{1}{\sqrt{2}}\left(\frac{j_d}{m_d}\right)\lambda r_{200}$$

$$\approx 8.8h^{-1}\,\mathrm{kpc}\left(\frac{\lambda}{0.05}\right)\left(\frac{V_c}{250\,\mathrm{km\,s^{-1}}}\right)\left[\frac{H}{H_0}\right]^{-1}\left(\frac{j_d}{m_d}\right), \tag{12}$$

and

$$\Sigma_0 \approx 4.8\times 10^{22} h\,\mathrm{cm^{-2}} m_H \left(\frac{m_d}{0.05}\right)\left(\frac{\lambda}{0.05}\right)^{-2}$$

$$\times\left(\frac{V_c}{250\,\mathrm{km\,s^{-1}}}\right)\left[\frac{H(z)}{H_0}\right]\left(\frac{m_d}{j_d}\right)^2, \tag{13}$$

where m_H is the mass of a hydrogen atom.

approximate the distribution of λ by

$$p(\lambda)\,d\lambda = \frac{1}{\sqrt{2\pi}\sigma_\lambda}\exp\left[-\frac{\ln^2(\lambda/\bar{\lambda})}{2\sigma_\lambda^2}\right]\frac{d\lambda}{\lambda}, \qquad (15)$$

where $\bar{\lambda} = 0.05$ and $\sigma_\lambda = 0.5$. This function is a good fit to the *N*-body results of Warren et al. (1992; see also Cole & Lacey 1996;

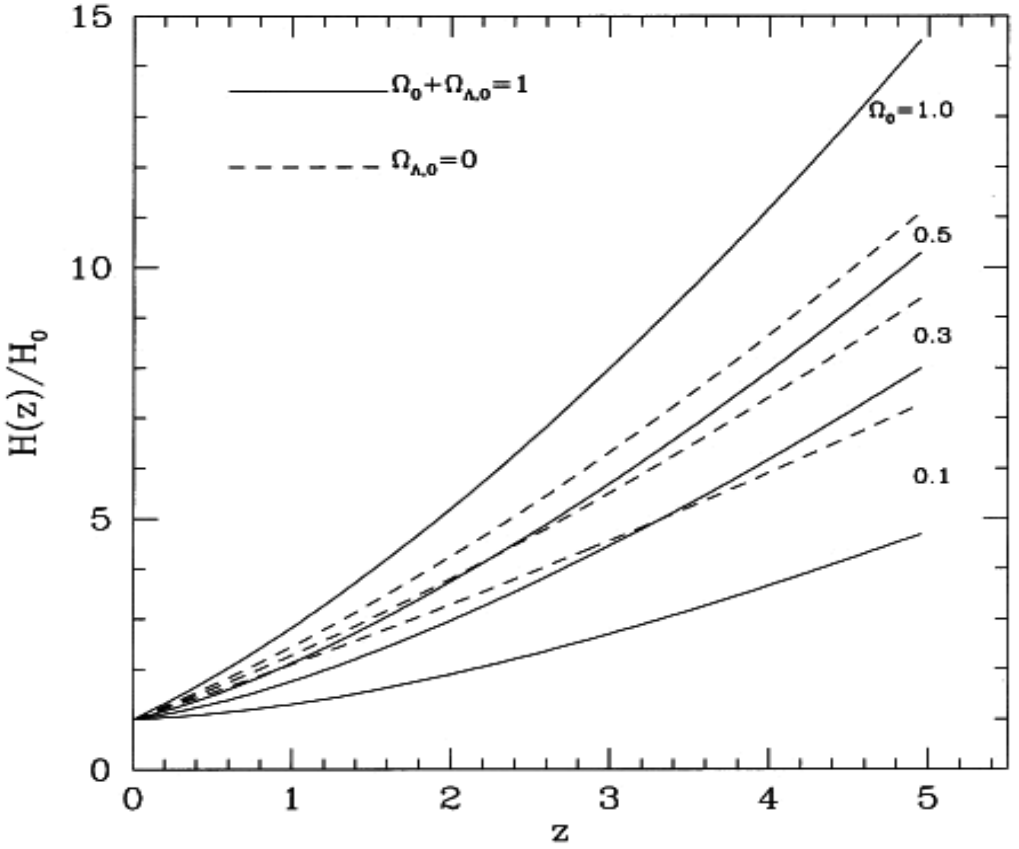

Figure 1. The Hubble constant (in units of its present value) as a function of redshift for flat ($\Omega_0 + \Omega_{\Lambda,0} = 1$) and open models with various Ω_0.

Sizes of Disk Galaxies and their Evolution

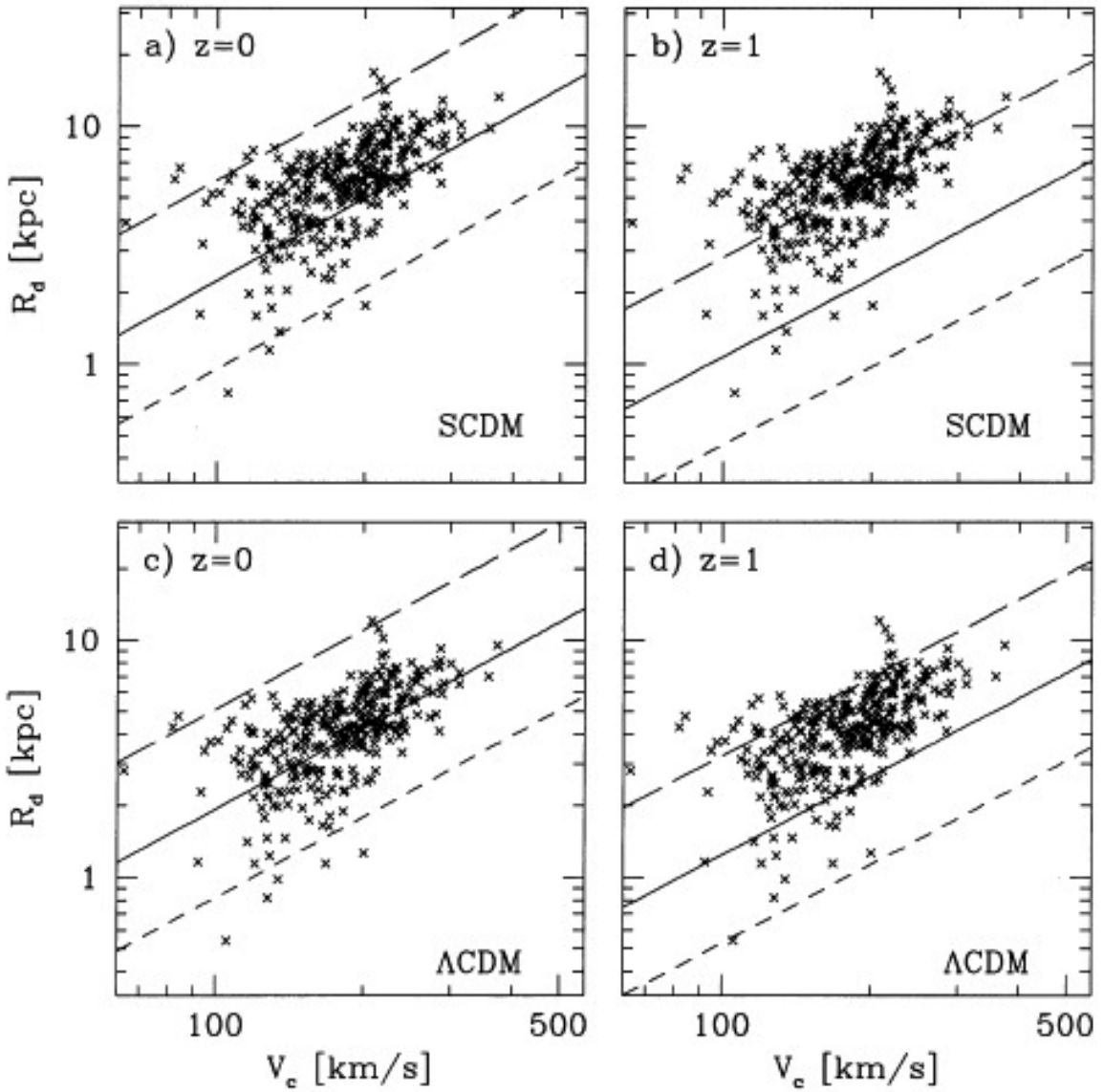

Figure 4. Model predictions for R_d as a function of V_c for stable discs assembled at $z = 0$ and at $z = 1$ in the SCDM and ΛCDM models. The solid lines give the relations for critical discs when $m_d = 0.05$, while short-dashed lines give the corresponding relations for $m_d = 0.025$. Stable discs must lie above the line for the relevant value of m_d. The long-dashed lines correspond to $m_d = j_d$ and $\lambda = 0.1$; at most 10 per cent of discs should lie above these lines. The data points are the observational results of Courteau (1996, 1997) for a sample of nearby normal spirals.

Predicted Rotation Curves: dependence on parameters

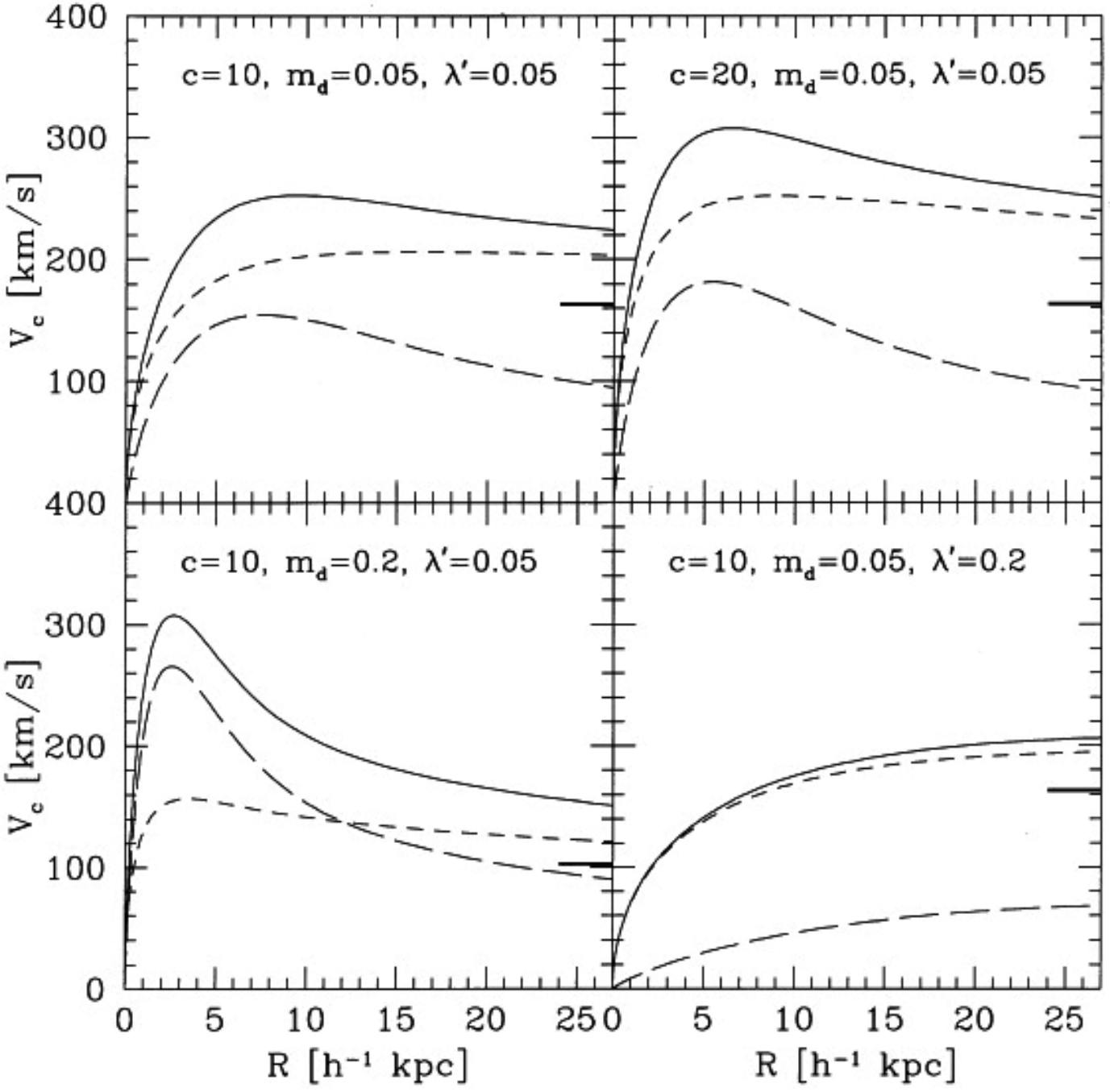

Theoretically predicted Tully-Fisher Relations

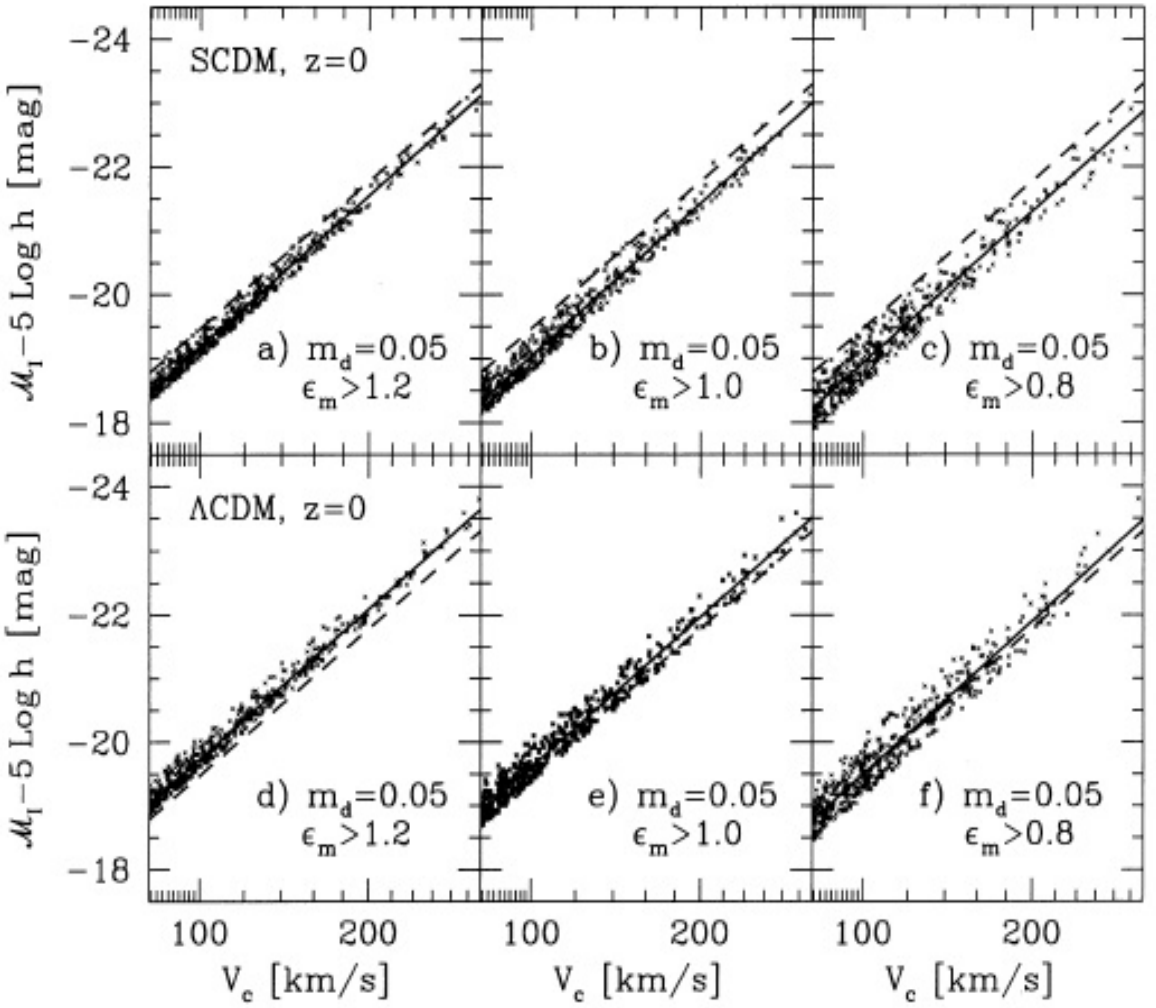

Figure 6. Tully–Fisher (TF) relations for stable discs at $z = 0$ in the SCDM and ΛCDM cosmogonies. Monte Carlo samples of the predicted luminosity–rotation velocity distribution are shown for three choices of ϵ_m. We have converted stellar mass (in the model) into I-band luminosity using $\Upsilon = 1.7h$ (Bottema 1997). The solid lines give the linear regressions of absolute magnitude against log V_c. The dashed lines show the observed TF relation as given by Giovanelli et al. (1997).

DISK GALAXY FORMATION IN COSMOLOGICAL HYDRODYNAMICAL SIMULATIONS

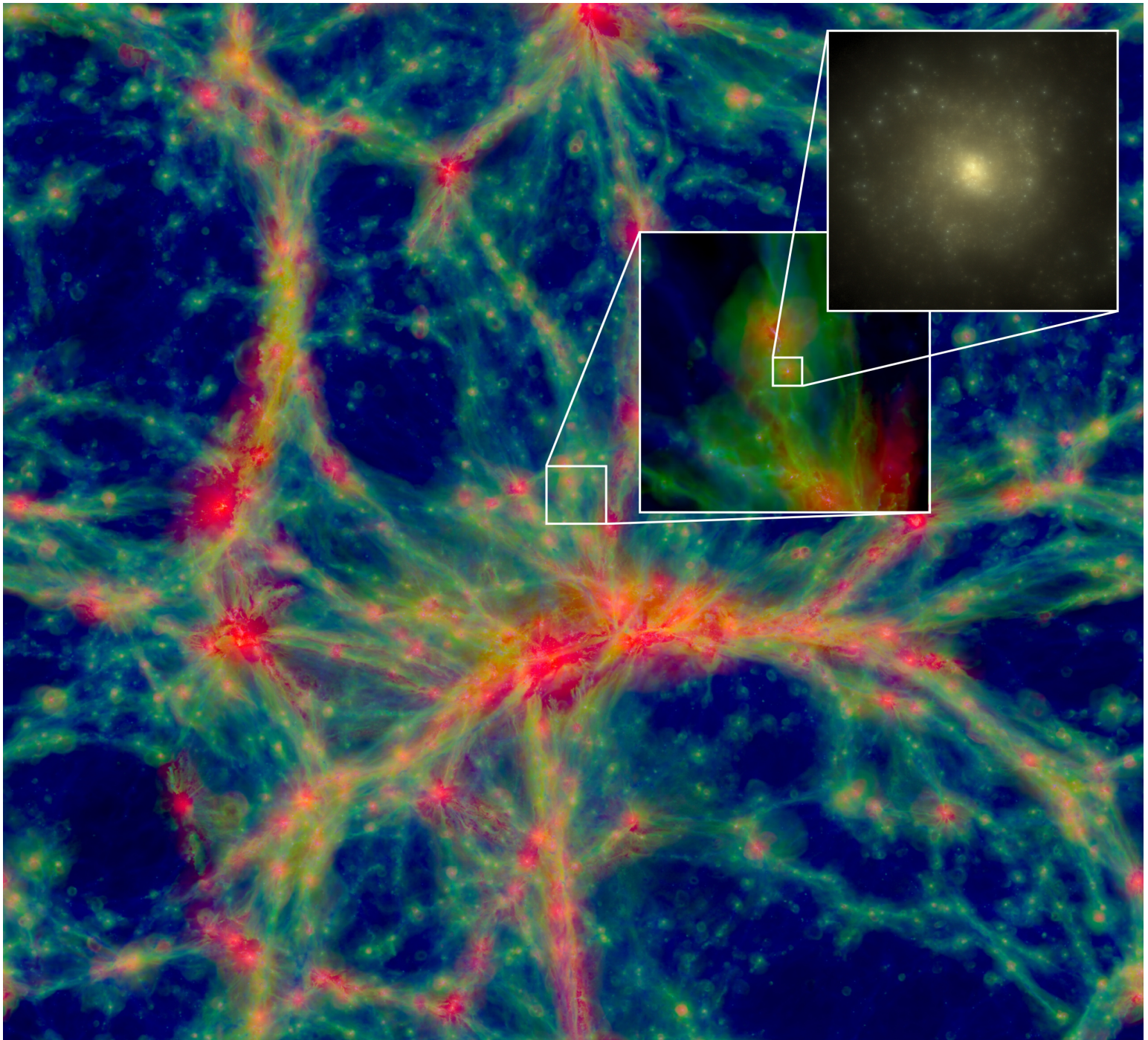

N-body hydrodynamical simulations and the "Angular Momentum Catastrophe"

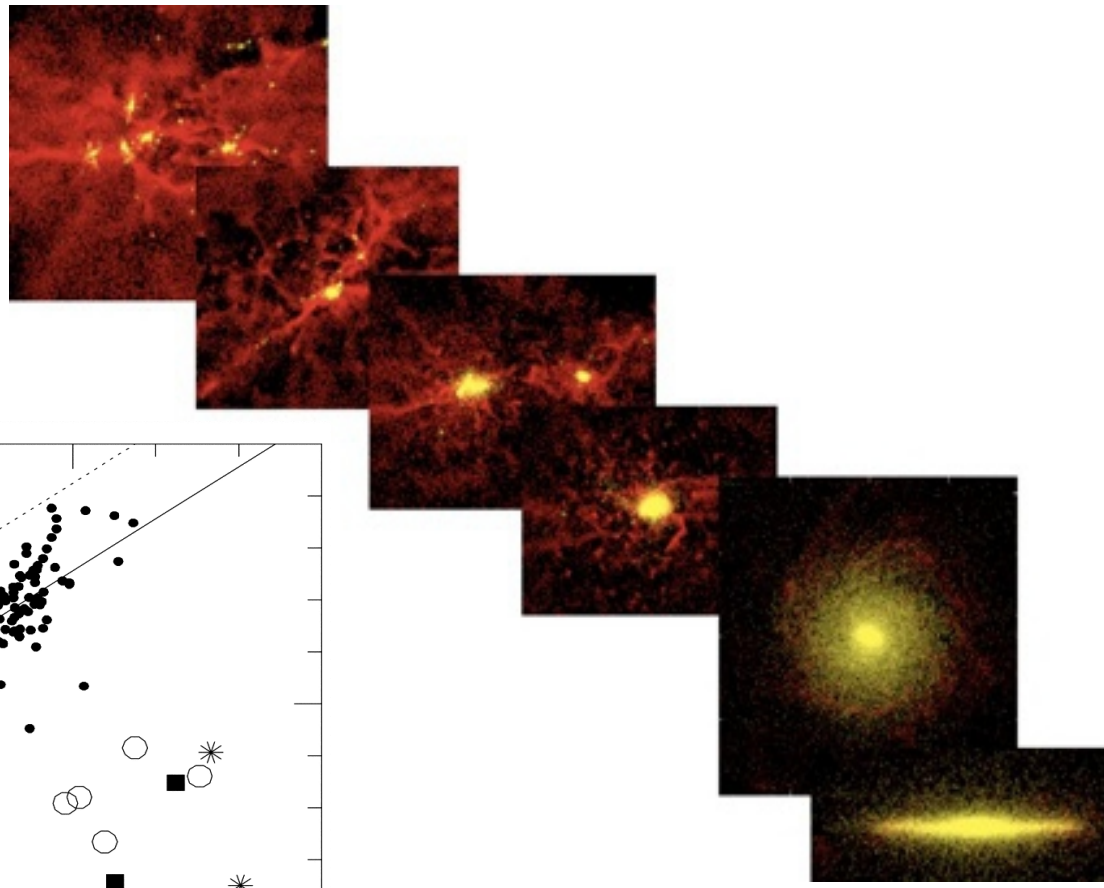

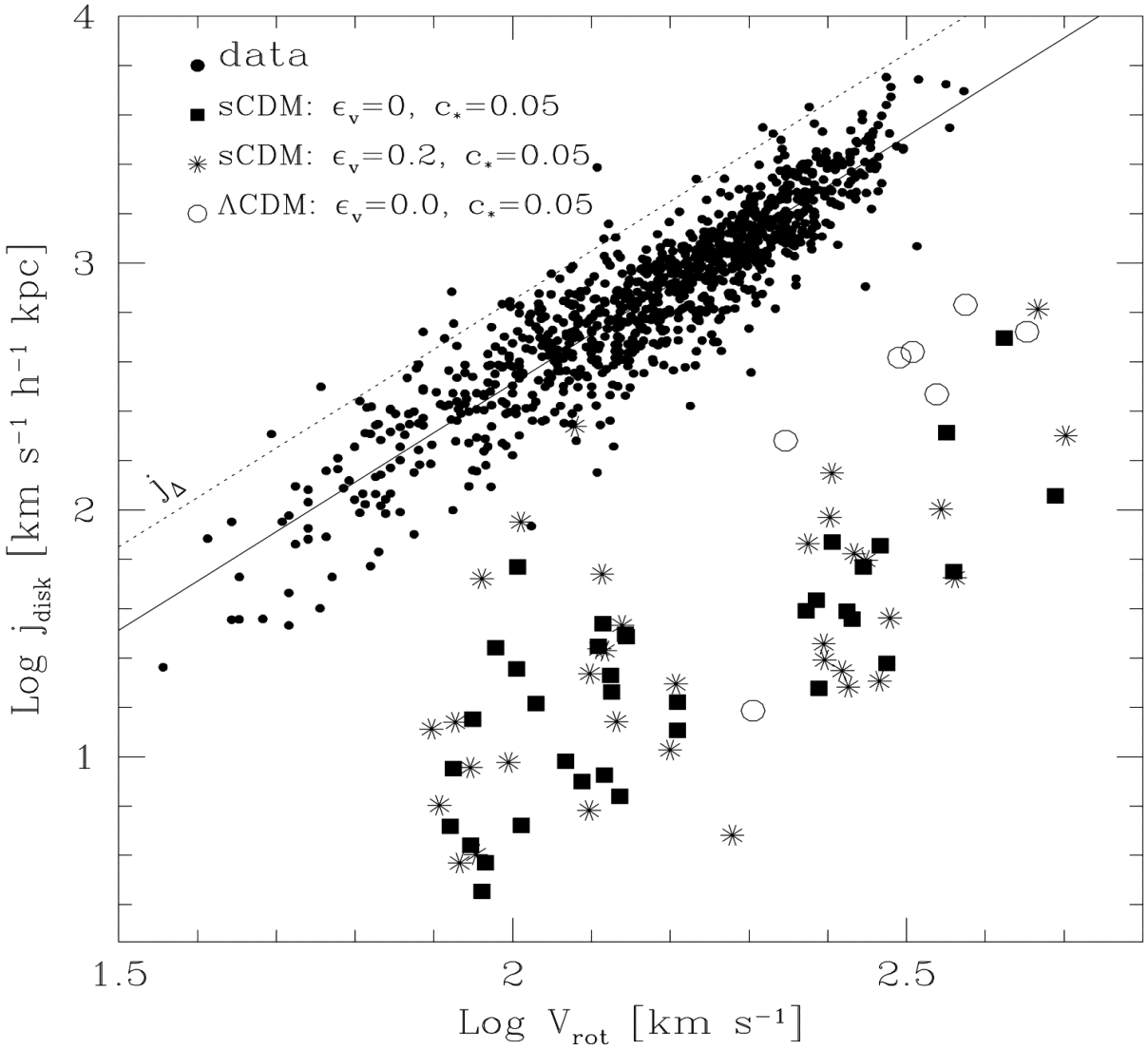

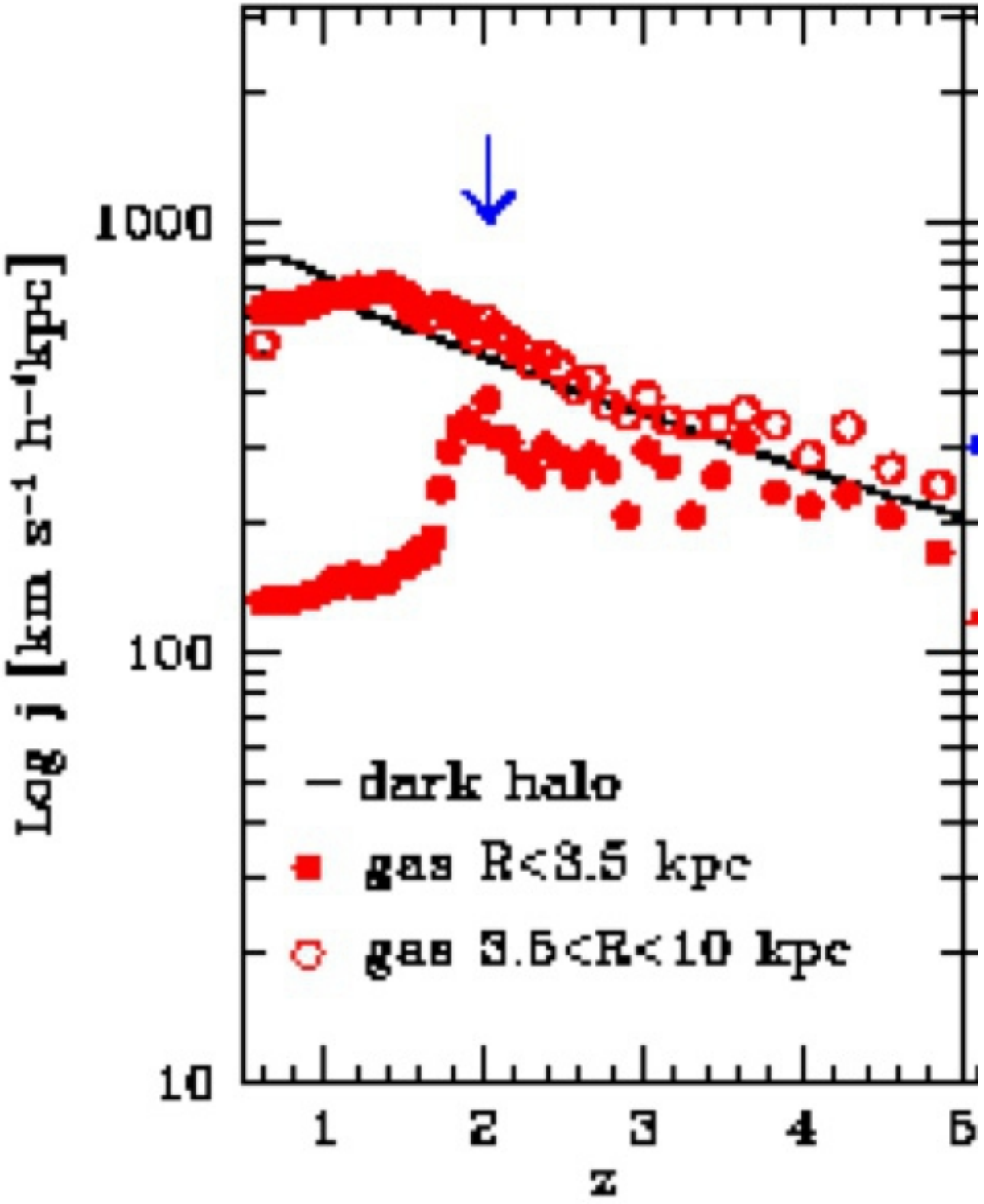

The gas loses angular momentum to the dark matter during merging events at high redshifts.

Effects of Feedback. Zavala et al 08

No FB

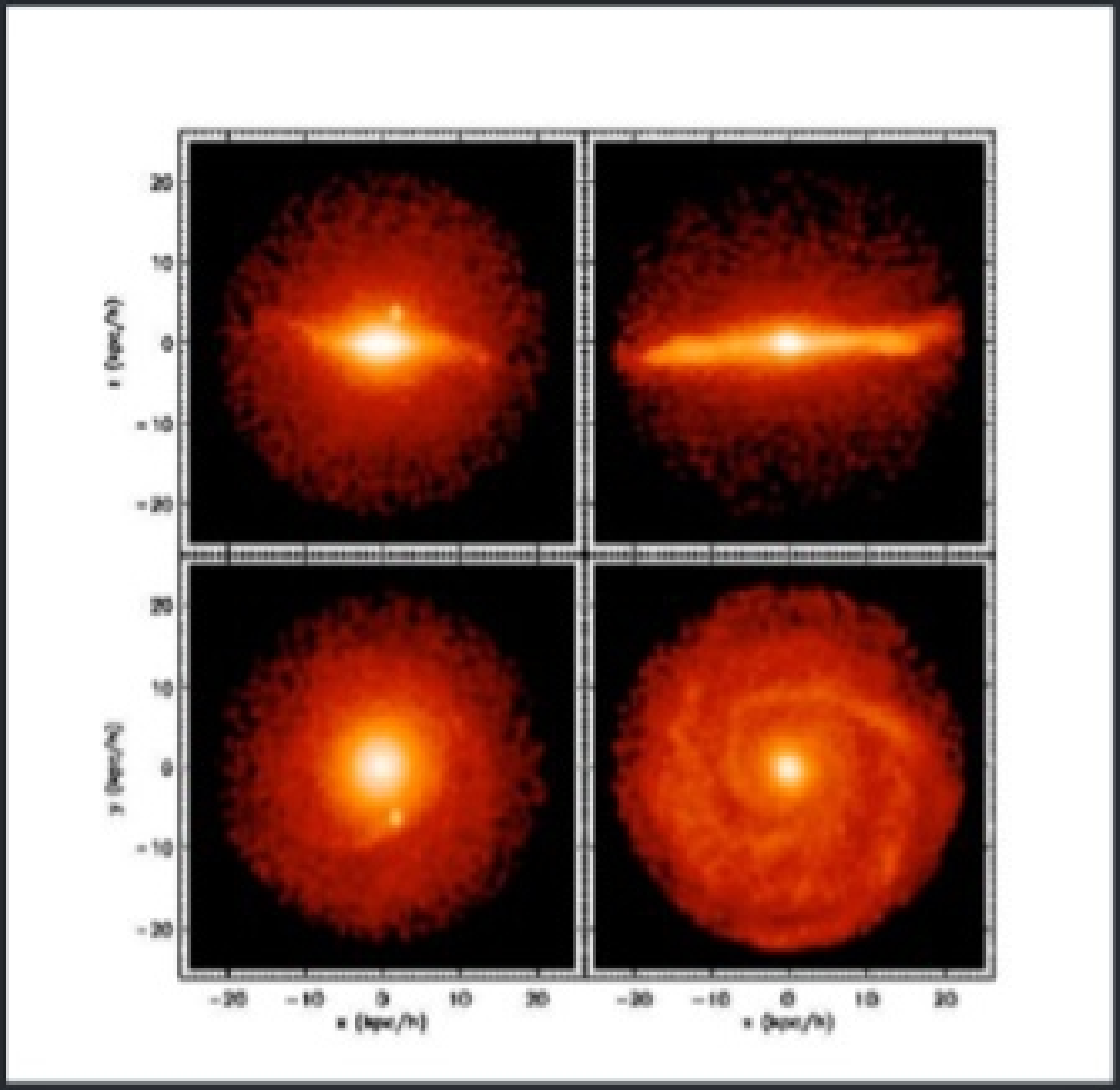

FB on.

Effect of different supernova feedback implementations on the predicted rotation curves.